0040993 61

START 9513358.1419

ENGINEERING DATA TRANSMITTAL

Page 1 of 1

1. EDT 609096

2. To: (Receiving Organization) Distribution	3. From: (Originating Organization)	4. Related EDT No.: N/A
5. Proj./Prog./Dept./Div.: OM582	6. Cog. Engr.: T. Lopez	7. Purchase Order No.: N/A
8. Originator Remarks:		9. Equip./Component No.: N/A
		10. System/Bldg./Facility: N/A
11. Receiver Remarks:		12. Major Assm. Dwg. No.: N/A
		13. Permit/Permit Application No.: N/A
		14. Required Response Date:

15. DATA TRANSMITTED

(A) Item No.	(B) Document/Drawing No.	(C) Sheet No.	(D) Rev. No.	(E) Title or Description of Data Transmitted	(F) Approval Designator	(G) Reason for Transmittal	(H) Originator Disposition	(I) Receiver Disposition
1	WHC-SD-WM-RPT-116	0	0	Summary of FY 1994	L/AE	2	1	
				Raman Spectroscopy				
				Technology Cold Test				
				Activities				

16. KEY

Approval Designator (F)	Reason for Transmittal (G)		Disposition (H) & (I)	
E, S, Q, D or N/A (see WHC-CM-3-5, Sec.12.7)	1. Approval	4. Review	1. Approved	4. Reviewed no comment
	2. Release	5. Post-Review	2. Approved w/comment	5. Reviewed w/comment
	3. Information	6. Dist. (Receipt Acknow. Required)	3. Disapproved w/comment	6. Receipt acknowledged

17. SIGNATURE/DISTRIBUTION (See Approval Designator for required signatures)

(G) Reason	(H) Disp.	(J) Name	(K) Signature	(L) Date	(M) MSIN	(J) Name	(K) Signature	(L) Date	(M) MSIN	(G) Reason	(H) Disp.
2	1	Cog.Eng.T. Lopez	[signature]	3-31-95	L5-55						
2	1	Cog. Mgr. W. D. Winkelman	[signature]	3-31-95	L5-55						
		QA									
		Safety									
		Env.									

18. T. Lopez [signature] 3-31-95 Signature of EDT Originator Date	19. Authorized Representative for Receiving Organization Date	20. W. D. Winkelman [signature] 3/31/95 Cognizant Manager Date	21. DOE APPROVAL (if required) Ctrl. No. [] Approved [] Approved w/comments [] Disapproved w/comments

BD-7400-172-2 (04/94) GEF097

INSTRUCTIONS FOR COMPLETION OF THE ENGINEERING DATA TRANSMITTAL

(USE BLACK INK OR TYPE)

DRAFT

BLOCK	TITLE	
(1)*	EDT	• Pre-assigned EDT number.
(2)	To: (Receiving Organization)	• Enter the individual's name, title of the organization, or entity (e.g., Distribution) that the EDT is being transmitted to.
(3)	From: (Originating Organization)	• Enter the title of the organization originating and transmitting the EDT.
(4)	Related EDT No.	• Enter EDT numbers which relate to the data being transmitted.
(5)*	Proj./Prog./Dept./Div.	• Enter the Project/Program/Department/Division title or Project/Program acronym or Project Number, Work Order Number or Organization Code.
(6)*	Cognizant Engineer	• Enter the name of the individual identified as being responsible for coordinating disposition of the EDT.
(7)	Purchase Order No.	• Enter related Purchase Order (P.O.) Number, if available.
(8)*	Originator Remarks	• Enter special or additional comments concerning transmittal, or "Key" retrieval words may be entered.
(9)	Equipment/Component No.	• Enter equipment/component number of affected item, if appropriate.
(10)	System/Bldg./Facility	• Enter applicable system, building or facility number, if appropriate.
(11)	Receiver Remarks	• Enter special or additional comments concerning transmittal.
(12)	Major Assm. Dwg. No.	• Enter applicable drawing number of major assembly, if appropriate.
(13)	Permit/Permit Application No.	• Enter applicable permit or permit application number, if appropriate.
(14)	Required Response Date	• Enter the date a response is required from individuals identified in Block 17 (Signature/Distribution).
(15)*	Data Transmitted	
	(A)* Item Number	• Enter sequential number, beginning with 1, of the information listed on EDT.
	(B)* Document/Drawing No.	• Enter the unique identification number assigned to the document or drawing being transmitted.
	(C)* Sheet No.	• Enter the sheet number of the information being transmitted. If no sheet number, leave blank.
	(D)* Rev. No.	• Enter the revision number of the information being transmitted. If no revision number, leave blank.
	(E) Title or Description of Data Transmitted	• Enter the title of the document or drawing or a brief description of the subject if no title is identified.
	(F)* Approval Designator	• Enter the appropriate Approval Designator (Block 15). Also, indicate the appropriate approvals for each item listed, i.e., SQ, ESQ, etc.
	(G) Reason for Transmittal	• Enter the appropriate code to identify the purpose of the data transmittal (see Block 16).
	(H) Originator Disposition	• Enter the appropriate disposition code (see Block 16).
	(I) Receiver Disposition	• Enter the appropriate disposition code (see Block 16).
(16)	Key	• Number codes used in completion of Blocks 15 (G), (H), and (I), and 17 (G), (H) (Signature/Distribution).
(17)	Signature/Distribution	
	(G) Reason	• Enter the code of the reason for transmittal (Block 16).
	(H) Disposition	• Enter the code for the disposition (Block 16).
	(J) Name	• Enter the signature of the individual completing the Disposition 17 (H) and the Transmittal.
	(K)* Signature	• Obtain appropriate signature(s).
	(L)* Date	• Enter date signature is obtained.
	(M)* MSIN	• Enter MSIN. Note: If Distribution Sheet is used, show entire distribution (including that indicated on Page 1 of the EDT) on the Distribution Sheet.
(18)	Signature of EDT Originator	• Enter the signature and date of the individual originating the EDT (entered prior to transmittal to Receiving Organization). If the EDT originator is the cognizant engineer, sign both Blocks 17 and 18.
(19)	Authorized Representative for Receiving Organization	• Enter the signature and date of the individual identified by the Receiving Organization as authorized to approve disposition of the EDT and acceptance of the data transmitted, as applicable.
(20)*	Cognizant Manager	• Enter the signature and date of the cognizant manager. (This signature is authorization for release.)
(21)*	DOE Approval	• Enter DOE approval (if required) by signature or control number that tracks the approval to a signature, and indicate DOE action.

*Asterisk denote the required minimum items check by Configuration Documentation prior to release; these are the minimum release requirements.

9513358.1420

WHC-SD-WM-RPT-116
Revision 0

Summary of FY 1994 Raman Spectroscopy Technology Cold Test Activities

Prepared for the U.S. Department of Energy
Office of Environmental Restoration and
Waste Management

Westinghouse
Hanford Company Richland, Washington

Hanford Operations and Engineering Contractor for the
U.S. Department of Energy under Contract DE-AC06-87RL10930

APR 1995
RECEIVED
EDMC

Approved for Public Release

THIS PAGE INTENTIONALLY
LEFT BLANK

9513358.1421

RELEASE AUTHORIZATION

Document Number:	WHC-SD-WM-RPT-116, Rev. 0
Document Title:	SUMMARY OF FY 1994 RAMAN SPECTROSCOPY TECHNOLOGY COLD TEST ACTIVITIES
Release Date:	4/3/95

This document was reviewed following the procedures described in WHC-CM-3-4 and is:

APPROVED FOR PUBLIC RELEASE

WHC Information Release Administration Specialist:

Chris Willingham

C. Willingham 4/3/95

TRADEMARK DISCLAIMER. Reference herein to any specific commercial product, process, or service by trade name, trademark, manufacturer, or otherwise, does not necessarily constitute or imply its endorsement, recommendation, or favoring by the United States Government or any agency thereof or its contractors or subcontractors.

This report has been reproduced from the best available copy. Available in paper copy and microfiche. Printed in the United States of America. Available to the U.S. Department of Energy and its contractors from:

U.S. Department of Energy
Office of Scientific and Technical Information (OSTI)
P.O. Box 62
Oak Ridge, TN 37831
Telephone: (615) 576-8401

Available to the public from: U.S. Department of Commerce
National Technical Information Service (NTIS)
5285 Port Royal Road
Springfield, VA 22161
Telephone: (703) 487-4650

THIS PAGE INTENTIONALLY
LEFT BLANK

9513358.1422

SUPPORTING DOCUMENT

1. Total Pages ~~34~~ 102

2. Title	3. Number	4. Rev No.
Summary of FY 1994 Raman Spectroscopy Technology Cold Test Activities.	WHC-SD-WM-RPT-116	0

5. Key Words	6. Author
Raman, Fiber Optic, Spectroscopy, Lasers, Probes, Hot Cell, Screening, Characterization.	Name: T. Lopez Signature Organization/Charge Code OM582/H2CAA

7. Abstract

This report documents the development, optimization, and feature testing of a Raman Spectroscopy Characterization Tool in a cold cell environment. The LLNL supplied Raman System was used to evaluate fiber optic probes and to obtain spectra from tank waste simulants.

8. RELEASE STAMP

OFFICIAL RELEASE BY WHC
DATE APR 06 1995
Sta. 31

THIS PAGE INTENTIONALLY
LEFT BLANK

9513358.1423

WHC-SD-WM-RPT-116, Rev 0

Summary of FY 1994 Raman Spectroscopy Technology Cold Test Activites

T. Lopez
F. R. Reich
J. G. Douglas

March, 1995

THIS PAGE INTENTIONALLY
LEFT BLANK

9513358.1424

Table of Contents

1.0 INTRODUCTION 1-1

2.0 COLD TEST SYSTEM DESCRIPTION 2-1
- 2.1 Raman Spectroscopy Cold Test System 2-1
  - 2.1.1 Lasers 2-1
  - 2.1.2 CCD Detector Array and Driver Electronics 2-3
  - 2.1.3 Spectrometer 2-3
  - 2.1.4 Computer and Software Control System 2-3
- 2.2 Cold Test System Issues 2-4
  - 2.2.1 Cabinet Air Flow/Pressure 2-4
  - 2.2.2 Cabinet Air Temperature 2-6
  - 2.2.3 Doubled Nd:YAG 532nm Laser Stability 2-6
  - 2.2.4 Miscellaneous Observations 2-6
- 2.3 Fiber-Optic Probes 2-7
  - 2.3.1 Chisel Tip Probe 2-7
  - 2.3.2 Flat Face Probes 2-8
  - 2.3.3 NIR Diffuse-Reflectance Probe 2-8
  - 2.3.4 Co-Axial Probe 2-11
  - 2.3.5 Fiber-Optic Filters 2-11
- 2.4 Data Acquisition and Processing Software 2-11
  - 2.4.1 Spectrometer Set-up Software 2-12
  - 2.4.2 Data Acquisition Software 2-12
  - 2.4.3 Data Processing Software 2-13
- 2.5 Software Issues 2-14

3.0 GENERIC PROCEDURES 3-1
- 3.1 Hardware Setup 3-1
  - 3.1.1 Detector Setup 3-1
  - 3.1.2 Laser Startup 3-1
  - 3.1.3 Fiber-Optic Connections 3-1
  - 3.1.4 Probe Configuration 3-2
  - 3.1.5 Sample Preparation 3-2
  - 3.1.6 Probe/Sample Environment 3-2
  - 3.1.7 Spectrometer Settings 3-2
  - 3.1.8 Computer/Software Settings 3-2
- 3.2 Wavelength Calibration 3-3
- 3.3 Data Acquisition 3-5

THIS PAGE INTENTIONALLY
LEFT BLANK

4.0 RAMAN DATA 4-1
4.1 Chemical Standards 4-1
4.2 Signal-to-Noise Measurements 4-2
4.2.1 S/N Processing 4-2
4.2.2 System Repeatability and Sample Repeatability S/N Measurements . . . 4-4
4.3 Probe Comparison Tests 4-5
4.3.1 Purpose 4-5
4.3.2 Comparison Data 4-6
4.4 Tank Waste Simulant Spectra 4-8
4.4.1 Tank Waste Simulant Diffuse-Reflectance Studies 4-9
4.4.2 Tank Waste Simulant Raman Spectra 4-11

5.0 REFERENCES 5-1

APPENDIX A A-1

APPENDIX B B-1

APPENDIX C C-1

APPENDIX D D-1

APPENDIX E E-1

THIS PAGE INTENTIONALLY
LEFT BLANK

9513358.1426

List of Figures

Figure 1-1. Progressive Technology Development Diagram. 1-2
Figure 2-1. LLNL Raman System Layout. 2-2
Figure 2-2. Internal Layout of LLNL Raman System. 2-5
Figure 2-3. Fiber-Optic Probe Designs 2-9
Figure 2-4. WSRC Probe Design. 2-10
Figure 3-1. Neon Spectrum at 600nm Center Wavelength. 3-4
Figure 4-1. Typical Regions of Sodium Nitrate Spectrum Used for S/N Calculations. 4-3
Figure 4-2. Example Spectrum for Calculating Silica Response Factor. 4-6
Figure 4-3. Probe Comparison of Dark-Charge/White-Light Corrected Sodium Nitrate Spectra. 4-7
Figure 4-4. Tank Waste Simulant Diffuse-Reflectance Spectra. 4-10
Figure 4-5. Raman Spectrum of BY-104 Simulant: Oxyanion Region. 4-12
Figure 4-6. Raman Spectra of SY-101 Simulant and SY-101 Tank Waste: Oxyanion Region 4-13
Figure 4-7. Raman Spectra of SY-101 Simulant and SY-101 Tank Waste: Ferrocyanide/ CH-Stretch Region 4-14
Figure 4-8. Raman Spectrum of T-Plant Top Simulant: Oxyanion Region. 4-16
Figure 4-9. Raman Spectrum of T-Plant Top Simulant: Ferrocyanide and CH-Stretch Region 4-16
Figure 4-10. Raman Spectrum of T-Plant Bottom Simulant: Oxyanion Region 4-17
Figure 4-11. Raman Spectrum of T- Plant Bottom Simulant: Ferrocyanide and CH-Stretch Regions. 4-18
Figure A-1. LLNL System Diagram. A-6
Figure C-1. Laser Bandpass and Long-Pass Filter Characteristics for 514.5-nm Excitation. . . C-7
Figure C-2. Laser Bandpass and Long-Pass Filter Characteristics for 532.2-nm Excitation. . . C-8
Figure C-3. Probe Optical-Filter Luminescence upon Laser Excitation. C-9

List of Tables

Table 2-1. Raman Data Acquisition/Processing Functions and Associated Software. 2-13
Table 3-1. Calibration Parameters, Typical Values. 3-5
Table 3-2. Spectral Data Collected. 3-6
Table 4-1. Comparison Summary. 4-8
Table 4-2. Experimental Conditions for Simulant Diffuse-Reflectance Spectra. 4-11
Table 4-3. Prominent peaks found in SY-101 simulant and tank waste and Raman spectra. . 4-14
Table A-1. Specifications for Raman System Cabinet. A-4
Table A-2. Specifications for Raman Computer System. A-7
Table A-3. Specifications for Raman System Laser A-8
Table A-4. Specifications for Raman System Spectrograph. A-9
Table A-5. Specifications for Raman System CCD Detector. A-11
Table A-6. Specifications for Raman System Fiber-Optic Interface. A-12
Table A-7. Specifications for Raman System Liquid-Nitrogen Auto-Filler System. A-13
Table C-1. 532 Long-Wave Pass Optical Filter. C-3
Table C-2. 532 Laser Band-Pass Optical Filter. C-4
Table C-3. Transmission Characteristics for Fiber-Optic Raman Probe Filters. C-6
Table C-4. Experimental Conditions for Determining Raman Probe Filter Transmission Characteristics. C-7
Table E-1. BY-104 Salt-Cake Simulant. E-4
Table E-2. Composition of T Plant Top Simulant. E-5
Table E-3. Composition of T Plant Bottom Simulant. E-6
Table E-4. Composition of SY-101 Simulant. E-7

EXECUTIVE SUMMARY

This report documents the development, optimization, and feature testing of a Raman spectroscopy characterization tool in a non-radioactive environment. The Department of Energy's Offices of Technology Development and Tank Waste Remediation Systems are jointly sponsoring development of Raman technology (1) to obtain safety-related information about the ferrocyanide and organic content of tank waste, and (2) to reduce tank waste characterization costs through rapid chemical screening of tank waste.

The Raman system used for this work was designed by Lawrence Livermore National Laboratory (LLNL), specifically for use in hot-cell facilities where air-borne contamination is an issue. The components were packaged in an air-tight cabinet and included:

- an argon-ion laser,
- a liquid-nitrogen cooled charge-coupled device,
- a single grating, Czerny-Turner f/4.0 spectrograph,
- a 386-based computer system, and
- a HEPA-filtered air ventilation system.

In operating the Raman system, several issues related to the system components and their operation were identified. Significant design issues include:

- The laser air-cooling system under-pressurizes the Raman cabinet so that the cabinet operates at a slight vacuum. The cabinet should be designed to operate at a slight over-pressure condition to keep air flowing out of cabinet penetrations and openings.
- The high heat dissipation of the argon-ion laser caused the spectrograph wavelength to drift. The cabinet temperature must be kept as constant as possible.

Four different sets of software were used to perform the different data acquisition and data processing functions needed to obtain and analyze Raman spectra. There are several software issues that remain to be addressed including:

- automation of data collection,
- automation of data processing, and
- integration of data collection and processing functions.

Several fiber optic probe designs were evaluated. These probes include:

- a Westinghouse Savannah River Company chisel tip probe,
- a LLNL six-around-one probe,
- a commercially available 36-around-one probe,
- a commercially available near-infrared diffuse-reflectance probe, and
- a commercially available co-axial probe.

Three factors were identified in selecting a fiber-optic probe design for remote Raman spectroscopy: (1) signal-to-noise performance, (2) the intensity of the probe's silica Raman

spectrum, and (3) the probe's collection efficiency. Of the five probes tested, the following conclusions were made:

- The flat-face probes are most efficient at getting light to the spectrometer as measured by the efficiency factor.
- The NIR diffuse-reflectance probes is least efficient, but has superieor S/N and silica peak ratio values.
- The flat-face probes and the chisel-tip probe have a significantly higher silica response than do the NIR diffuse-reflctance and co-axial probes.
- Multiple collection fiber probes are more efficient at collecting Raman-scattered light than single collection fiber probes.

Spectra were collected using BY-104, SY-101, T-Plant Top Sludge and T-Plant Bottom Sludge tank waste simulants to:

- determine how well the various probe types and laser excitation wavelengths would perform with materials similar to those of real tank wastes,
- determine the spectral absorption characterisitics of tank-waste-like materials, and
- determine what species could be detected in these materials.

Several important findings were made from the tank waste simulant tests:

(1) Diffuse reflectance studies revealed that the simulants exhibit strong absorbance in the 400nm to 600nm region. Operating at shorter wavelengths (above 600nm) may yield more Raman scattered light for collection.

(2) For the T-Plant simulants, the presence of sodium nickel ferrocyanide species is detectable at least as low as 0.84 weight per cent.

(3) In the oxyanion region, probes with low-silica-raman backgrounds produced the spectra most readily treated to remove the silica-Raman background signal.

(4) In the ferrocyanide and CH-stretch regions, the probe silica-Raman background is not as significant as it is in the oxyanion region.

1.0 INTRODUCTION

This report contains a summary of the FY 1994 Raman spectroscopy technology development and test work completed with non-radioactive materials in a non-radioactive environment. The Department of Energy's (DOE) offices of Technology Development (EM-30) and Tank Waste Remediation Systems (EM-30) are jointly sponsoring development of Raman technology to obtain chemical information from Hanford high-level radioactive waste (HLW) both in the hot-cell and in Hanford Site waste tanks. The principal drivers for this development effort are:

(1) to obtain safety-related information about the ferrocyanide and organic content of tank waste, and
(2) to reduce tank waste characterization costs through rapid chemical screening of tank waste.

The Raman spectroscopy work reported in this document was performed using pure reference materials and non-radioactive, simulated tank wastes in a non-radioactive test facility at the Hanford Site's 305 Building. As indicated in Figure 1-1, non-radioactive testing and development work is part of the total life cycle path being followed in the application of Raman spectroscopy technology to Hanford's HLW materials. The EM-50 Office of Technology Development is providing support for the development and optimization of the basic Raman system and system components. The EM-30 Tank Waste Safety and Tank Waste Remediation Systems programs at Hanford are supporting the application of this technology for hot-cell testing and deployment.

The need to rapidly and economically determine the molecular species of waste tank materials is the principal driver in the development and deployment of the Raman spectroscopy technology. Characterization data are needed to support safe tank farm operations and to support the development of the technologies and processes that will be required to stabilize and process the radioactive waste materials (Wodrich et al. 1994).

In the near-term, characterization needs have been dominated by data needs to support safe tank farm operations. Organic compounds were used in some separation processes and ferrocyanide compounds were used in the management of tank waste. The existence of these potential feuls mixed with possible oxidizers in the tanks raises the possibility of unsafe conditions (Postma et al. 1994). Over the longer term, data are needed to support technologies and processes that will be required to stabilize the radioactive wastes.

A remote, fiber optic, Raman spectroscopy probe may provide both qualitative and quantitative data for both hot-cell core measurements and in situ waste tank applications. In the current tank waste characterization process, waste cores are extracted from a tank and extruded in a hot-cell where sub-samples are selected for detailed chemical analyses. These methods require significant sample preparation and pretreatment and are labor intensive, time consuming, and result in the generation of secondary waste. As a hot-cell screening tool, a Raman spectroscopy probe will

Figure 1-1. Progressive Technology Development Diagram.

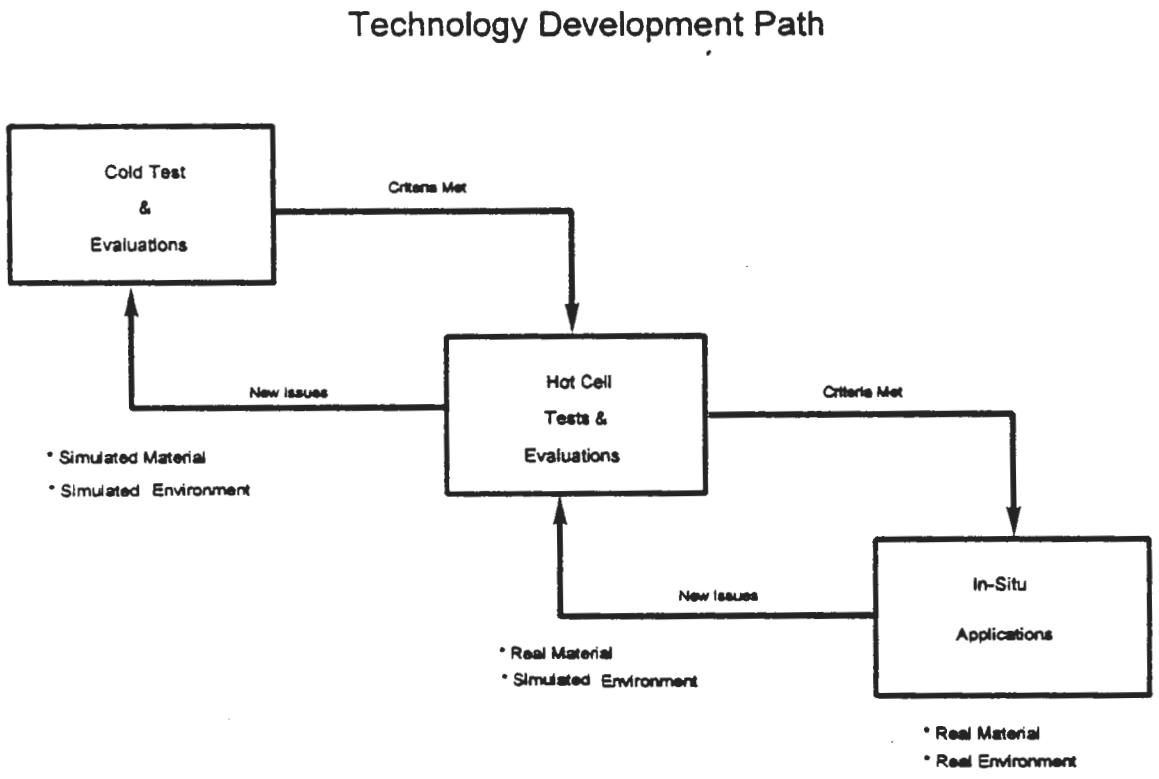

allow the rapid collection of characterization data, the reduction or elimination of sample preparation steps, and the subsequent reduction in the number of traditional chemical analyses. A hot-cell Raman probe may provide capability to quickly obtain species profiles along the axis of the core sample that are not possible with current methods. This species profile information may help reduce the number of sub-samples required for subsequent laboratory chemical analysis, thus reducing the total analysis cost for a core segment.

In situ applications are also being pursued with deployment systems that include the Light Duty Utility Arm (LDUA) and Cone Penetrometer systems. A remote Raman characterization probe could support both qualitative and quantitative analysis, reducing the need for waste extraction from a tank and hot-cell analysis. Its development as a characterization assessment tool for hot-cell and in situ characterization offers significant reduction in time, cost, and secondary waste generation; the complexity and cost of extracting this traditional analytical data provides the principal motivation for this technology.

2.0 COLD TEST SYSTEM DESCRIPTION

This section describes the hardware and software used to perform testing activities. Section 2.1 describes the spectroscopy system designed by Lawrence Livermore National Laboratory, the fiber-optic probes tested, and the fiber-optic filters used. Section 2.2 identifies design issues related to the system hardware and their operation. Section 2.3 describes the fiber-optic probes tested and fiber-optic filters used during testing activities. Section 2.4 identifies the various software packages used for data acquisition and spectral processing. Section 2.5 addresses software issues related to Raman spectral acquisition and data processing.

2.1 Raman Spectroscopy Cold Test System

The Raman system used for the FY 1994 cold testing in the 305 building was designed by Lawrence Livermore National Laboratory (LLNL), specifically for use in hot-cell facilities where air-borne contamination is an issue (see Appendix A). The major system components include:

- cabinet with electrical power bus
- argon-ion laser (monochromatic light source)
- spectrograph with fiber-optic interface
- charge-coupled device (CCD) detector array and driver electronics
- computer system
- high-efficiency particulate air- (HEPA) filtered air ventilation system
- fiber-optic bus panel

Appendix A contains additional system information, such as a detailed list of specifications for each system component. As shown in Figure 2-1, the LLNL Raman system is based on a dispersive spectrometer system with a remote fiber-optic probe and CCD detector in an enclosed cabinet. The CCD array detector provides a photo-sensitive surface. The fiber-optic probe allows the system to be used in remote sensing applications, such as in a hot-cell. An optical fiber conducts light from the laser to the sample surface; one or more collection fibers collect the Raman scattered light. The collected light is input to a spectrometer that creates a wavelength-dispersed image of the end of the optical fiber(s) on the surface of the CCD detector. A spectrum with a wavelength abscissa and intensity ordinate is created by summing together each column of pixels in the CCD's vertical dimension (orthogonal to the wavelength axis). The reader is directed to Appendix B for more data processing details.

2.1.1 Lasers

The LLNL Raman system was operated using two laser sources: a 200mw, air-cooled, argon-ion laser with a single emission line at 514.5nm (514.5309nm) and a 400mw, air-cooled, diode-pumped, doubled Neodymium:YAG (Nd:YAG) laser with a single emission line at 532nm (the manufacturer states the actual emission to be in the 532.17-532.1985 nm range). The argon-ion

Figure 2-1. LLNL Raman System Layout.

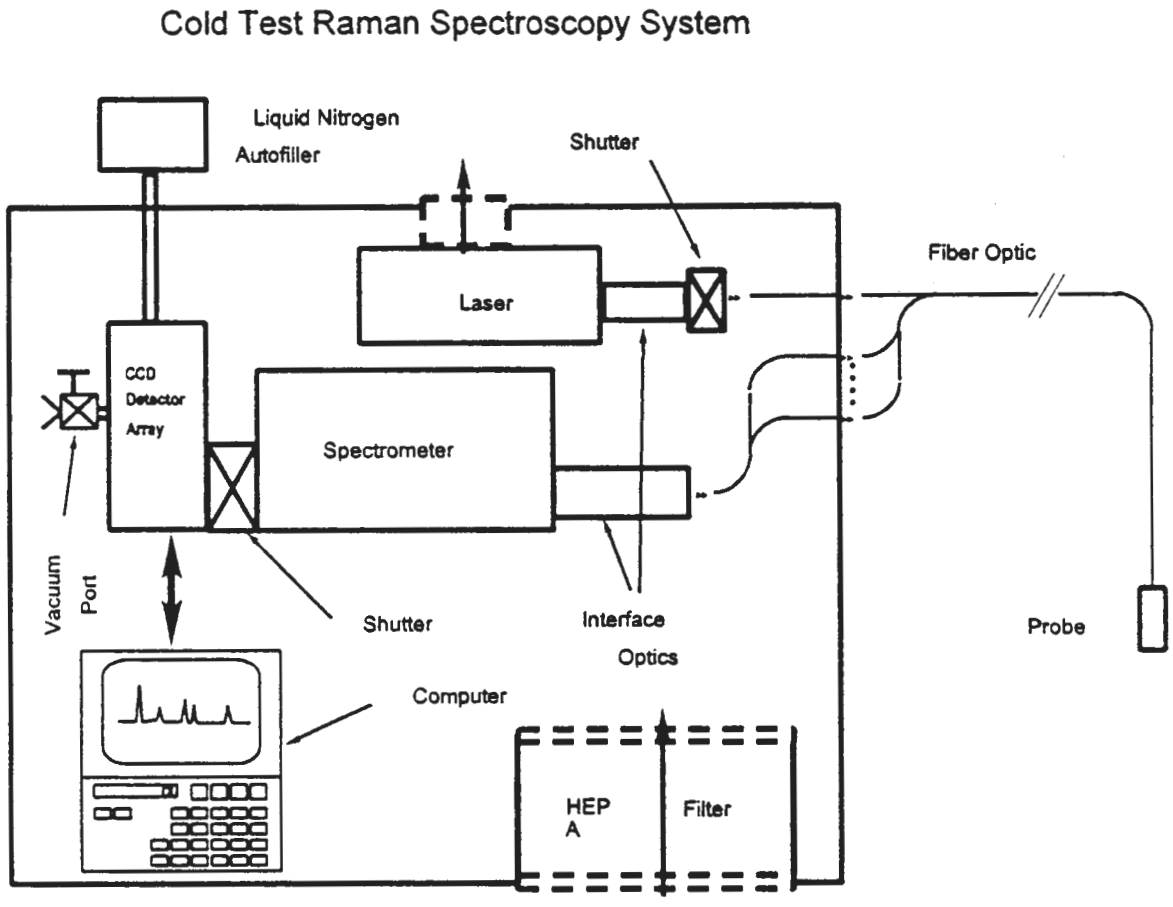

laser was an original part of the Raman system supplied by LLNL and was mounted in the cabinet as shown in Figure 2-1. The 532nm laser was added later by WHC but was not mounted in the air-tight cabinet. Both lasers were designed as light-tight packages with interfacing optics, including a shutter and fiber-optic interface, mounted on the laser head. The fiber-optic interface was terminated in an SMA-905 fiber-optic connector.

The argon-ion laser head also included a narrow band-pass filter that blocked the emission of super-radiant light and side bands located around the 514.5nm laser line. This was not required by the 532nm laser which had a very narrow, stable, single-mode emission line.

The argon-ion laser required about 30 minutes of warm-up time to reach a stable, full power condition. Any laser power changes required an additional 10-20 minute stabilization time.

2.1.2 CCD Detector Array and Driver Electronics

The LLNL Raman system used a two-dimensional CCD detector array with a liquid nitrogen cooled dewar. The CCD was a thinned, back-illuminated device with 1024x1024 picture elements (pixels), each pixel having a 24x24μm size. The liquid nitrogen cooling was originally selected over thermoelectric (TE) cooling because it produced less background noise than the same detector with TE cooling. The detector housing was mounted on the output port of the spectrograph with the detection surface of the CCD at the image plane of the spectrograph and the horizontal CCD axis parallel to the spectrograph's dispersion axis. The back-illuminated, thinned CCD has a superior (factor of 2 or better) quantum efficiency compared with conventional front-illuminated CCDs over the spectral range of 0.5 to 1.0μm. It was necessary to periodically evacuate the detector to re-establish the vacuum which insulated the dewar detector's outer housing. A temperature controller on the CCD control unit was used to maintain the CCD temperature at approximately -120° C. Higher temperatures (i.e.. -90° C and higher) resulted in a significant increase of thermal noise from the detector.

For all spectrometer operations, each vertical column of pixels on the CCD was summed ("binned") to produce a single intensity value for that column. For the spectroscopy work presented in Section 4.0, the CCD controller was set to bin approximately 400 rows of the central portion of the CCD which included the light from the dispersed image of the fiber-optic input. When combined with the horizontal scan of the CCD, this produces a reading of the spectral dispersion from the spectrograph. Upper and lower CCD areas were basically void of light and only contributed noise to the signal when they were included.

2.1.3 Spectrometer

The spectrograph was a Czerny-Turner f/4.0 imaging system. The spectrograph had three different, individually selectable gratings mounted on a turret. The mirrors had focal lengths of 250mm and 330mm that gave the spectrometer an apparent magnification of 1.3. A hand-held controller was used to remotely select the grating, spectrometer wavelength, and entrance slit width. With a 1200g/mm grating in first order and a 20μm entrance slit width, the spectrograph had a reciprocal linear dispersion of approximately 2.5 nm/mm. The spectrograph's fiber-optic interface provided an optical match between the fiber-optic which had a numerical aperature (NA) of 0.22 and the spectrometer's f/4.0 optics.

2.1.4 Computer and Software Control System

A 386-based computer was used to control the collection of data from the spectrometer CCD. The computer used a direct memory access (DMA) link for high-speed data readout from the CCD's controller system. All spectra were initially recorded on the computer system's hard disk

and then, after pre-processing, were transferred to high-density floppy disks for further processing and archival operations.

Each spectral data file contained a header where selected system and sample information were recorded and archived with the spectrum. This header information was copied to the headers of the data files that were generating during subsequent data processing steps.

The detector was operable with two different software packages;
(1) a vendor-supplied software package provided with the CCD detector system, and
(2) a custom software package supplied by Florida State University (FSU).

The FSU software was used as the chief "work-horse" to obtain Raman spectra. See Section 2.4 and Appendix B for additional information regarding data collection and processing software and data processing procedures. The vender-supplied software package contained several direct imaging functions with the two-dimensional CCD detector that are helpful in assessing the alignment of the detector to the spectrograph and in selecting the binning parameters.

2.2 Cold Test System Issues

Non-radioactive testing with the LLNL Raman system revealed a number of issues related to the system components and their operation. Appendix A contains a detailed description of this equipment.

2.2.1 Cabinet Air Flow/Pressure

The laser air-cooling system under-pressurizes the Raman cabinet so that the cabinet operates at a slight vacuum. This compromises the air-tightness of the cabinet and promotes the possible ingress of dust and (if in a radiation zone) air-borne radioactive contamination; the Raman system would be located in the hot-cell operating gallery where there is a potential for air-borne radioactive contamination.

The design of the laser air-cooling components is the cause of this problem. The air-cooled argon-ion laser requires a large flow of air for cooling the laser head and power supply. As indicated in Figure 2-2, air enters the bottom of the cabinet, flows up through the HEPA filter, and is then drawn past the laser power supply and through the laser head. The laser head is mounted directly against the upper surface of the cabinet through a duct assembly. A flexible air hose, with a squirrel-cage fan at its free end, is connected to the duct. The fan draws air out of the cabinet creating an under-pressure condition (slight vacuum relative to the room ambient air pressure) in the cabinet.

Figure 2-2. Internal Layout of LLNL Raman System.

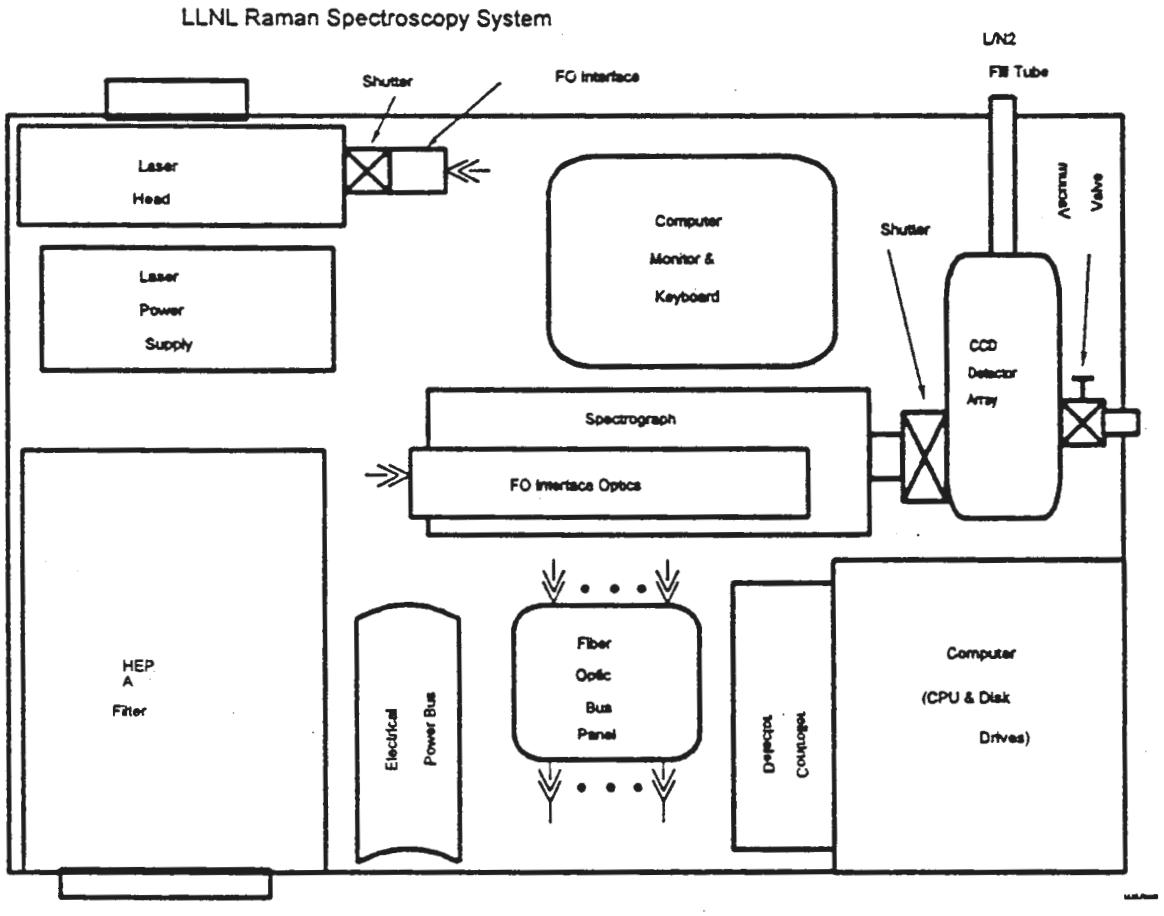

If a more efficient laser, such as a doubled Nd:YAG laser emitting at 532nm or a diode laser is used, then the air cooling requirements could be reduced. However, the placement of the fan still needs to be changed so that the cabinet operates at a slight over-pressure condition to keep air flowing out of cabinet penetrations and openings.

To complete routine maintenance operations, such as system alignment, evacuation of the CCD dewer, computer mainframe power control, etc., it was necessary to open the LLNL Raman system cabinet. This compromised the contamination-prevention design of the air-tight cabinet and HEPA filter system. This compromises the ability for maintenance/upgrading and for subsequent use outside of the hot-cell area after it has been used in a hot-cell campaign.

Most of these maintenance related issues can be solved by the use of remote design or sealed penetrations through the cabinet walls. The cabinet as it now exists provides filter air only to protect the optical components through extended use in optically hostile environments (air-borne dust and aerosols).

2.2.2 Cabinet Air Temperature

During prolonged periods of operation with the cabinet closed, the spectrograph wavelength was found to drift. A thermocouple temperature sensor was attached to the spectrograph and recorded a temperature rise that correlated with the on-set of spectrograph drift. Although there is a large flow of air through the cabinet, apparently most of the air flows directly from the HEPA filter through the laser head. As originally designed, there is very little air exchange around the other modules in the cabinet. A small muffin fan was placed in the upper corner of the cabinet to create a circular air flow around the spectrograph and monitor.

Although lasers with much lower heat dissipation will be used in future Raman systems (e.g. solid-state 532nm Nd:YAG lasers and 785-nm diode lasers), there will still be a need to keep the cabinet temperature as constant as possible.

2.2.3 Doubled Nd:YAG 532nm Laser Stability

The doubled Nd:YAG 532nm laser exhibited some intermittent stability problems where the laser would not lock on to a stable output mode of operation. It was necessary to attach a computer to the laser head and use a software-driven RS-232 link to force the system to re-calibrate. In some cases, it was necessary to lower the laser power level to achieve stability. After stability was achieved, the computer could be disconnected and the laser would continue its stable operation, even after turning the laser off and back on again.

The source of the instability was not found and this particular doubled Nd:YAG laser should be returned to the manufacturer for test and repair. In addition, a small portable computer with an RS-232 link should be available if these lasers continue to be used. Operating with the computer is not a normal operating condition for this laser, but it is the only way that the laser's power level can be adjusted. A computer was not furnished with the laser system, but the software control program was included.

2.2.4 Miscellaneous Observations

This section covers three miscellaneous observations regarding the LLNL Raman system; these observations include (1) a recurring problem with the argon-ion laser fuse blowing, (2) slow computer operation, and (3) computer monitor placement.

Argon-Ion Laser Fuse Problem: It was discovered that a 2-amp fuse in the argon-ion laser power supply would blow on occasion. The source of the fault was never determined.

Slow Computer Operation: The computation speed of the 386SX/16-based computer tended to slow data collection. The FSU *RCAL* software performs some spectral averaging and dark/white corrections as part of data collection, and these mathematical operations tended to slow data collection. To minimize the effect of real-time data processing on the rate at which spectra may be collected, it is recommended that the fastest computer system available be used for data collection.

Computer Monitor Placement: Optical alignment and focusing procedures require the user to be able to see the computer monitor (see Appendix D). The monitor is normally viewed from the front of the LLNL system cabinet; however, optical adjustments are performed from the *back* of the cabinet. Two approaches were used to overcome this short-coming. The first was to use two people to perform alignment — one to perform the alignment and the other to watch the monitor. The person viewing the monitor called out the results of an alignment operation to the person doing the aligning. This work-around performed poorly, especially when small adjustments (e.g. rotational tuning of the laser notch filter) resulted in large changes to the optical signal. The second, more satisfactory work-around, was to disconnect the Raman system monitor and substitute a spare computer monitor that faced the back of the LLNL cabinet. This allowed the adjuster to monitor the results of his efforts in real time. In designing any future self-contained Raman systems, it is recommended that the system computer monitor be positioned so that it may be easily viewed when performing optical alignment procedures.

2.3 Fiber-Optic Probes

To survive the hot-cell and waste-tank environments, fiber-optic probes must be both radiation and chemically resistant. The probes used in this work were constructed from commercially available, radiation-resistant, step-index, fused silica fibers with a polyimide buffer coating and chemically resistant jacketing. Proximal end, single fibers were terminated with SMA-905 connectors, as indicated above. The fiber-optic core diameters ranged from 200 to 400μm and had a numerical aperture of 0.22. (Since the interior of the LLNL system cabinet is not expected to sustain a significant dose rate, the fiber pigtails contained within the cabinet were made from non-radiation-resistant, communication-grade fiber.)

Several fiber-optic probe designs were evaluated. The various configurations of the fiber-optic probes are shown in Figure 2-3.

2.3.1 Chisel Tip Probe

Figure 2-4 shows the probe used for the bulk of the Raman cold testing; Westinghouse Savannah River Company (WSRC) supplied this probe. The probe has two fibers with a chisel-shaped

probe tip that causes the optical axis of the laser source and the detector collection fibers to cross. The window protects the fiber-optics from direct material contact, allowing the probe to be "mashed" into a solid/slurry. This "mashing" assures that the optimum sample position is always maintained by the outer surface of the window. The cross-over point is a function of the angle between the surfaces, fiber-optic numerical aperture, and the probe window thickness and refractive index. The protective window was epoxied to a screw-on holder which could be adjusted so that the optical cross-over occurred at the outer surface of the window. For a typical chisel tip probe, the cross-over point was set to occur about 0.75 mm from the apex of the chisel tip. At this setting, the sensing area for a 400µm, 0.22NA fiber probe is approximately 0.75mm in diameter.

The probe performance was evaluated with and without the optical laser band-pass and laser blocking filters, shown in Figure 2-4. The typical fiber length for an SRL probe was 6m and the probe was terminated with SMA-905 connectors (the chisel-tip end was also a modified SMA-905 fiber-optic connector housing). The optical filters (3.0mm diameter x 0.5mm thick) were inserted between the polished surfaces of SMA-905 connectors and the connectors finger tightened. These filters were also used with the NIR diffuse-reflectance probe described below.

2.3.2 Flat Face Probes

Figure 2-3 shows the major features of the two flat-face probes tested:

(1) a probe tip with six collector fibers around a central laser source fiber (6 around 1), and
(2) a probe tip with 36 collector fibers around a central laser fiber (36 around 1).

All optical fibers were low-water, radiation-resistant fibers (silica on silica, 0.22 N.A.) that had 200µm core diameters. There were no cover windows on either probe so the probe was manually positioned with an air space (lift-off distance) between the probe and sample surfaces (typically 3mm). No optical laser band-pass or laser blocking filters were used with either of these two probes.

2.3.3 NIR Diffuse-Reflectance Probe

The near-infrared (NIR) diffuse-reflectance probe was originally designed to collect diffuse reflectance from an optically scattering surface. This was a commercial probe from Polytec PI, Inc. (Auburn, MA). As shown in Figure 2-3, the probe head consisted of a hemispherical cavity

Figure 2-3. Fiber-Optic Probe Designs.

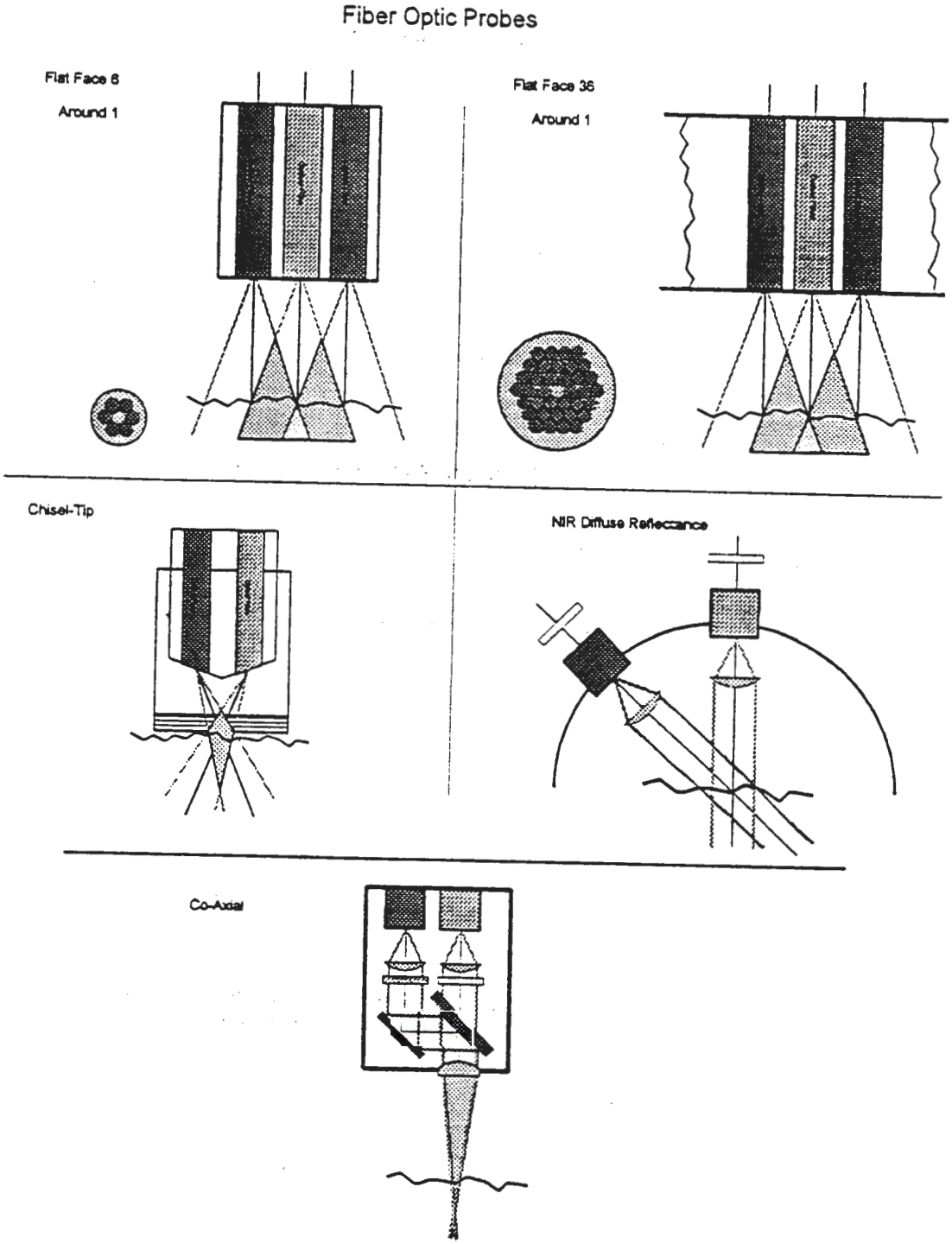

Figure 2-4. WSRC Probe Design.

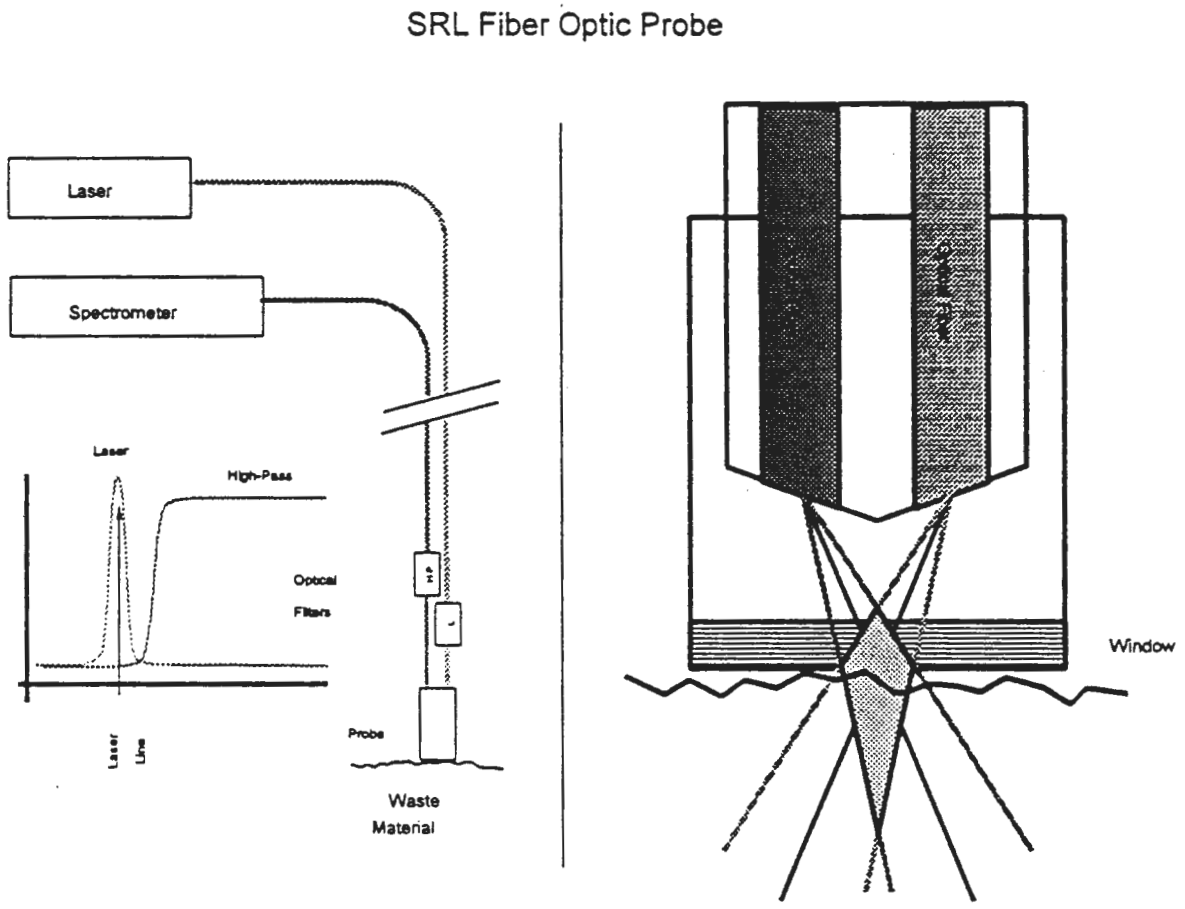

with two ports at 45° to each other; each port accommodated a fiber-optic/lens assembly. Each assembly consisted of a small adjustable lens and an SMA-905 fiber-optic connector. The lens position was used to control the spot size on the sample surface, which, for this testing, was set to approximately 9mm diameter.

For testing with the optical laser band-pass and long-pass filters, short fiber pigtails were connected to the probe head. The filters were then inserted between the pigtails and longer fiber-optic cables that were connected to the laser source and spectrograph.

2.3.4 Co-Axial Probe

The co-axial probe was a commercially built probe with an optical system that produced a focussed field of view, as indicated in Figure 2-3. The optical system and fiber cable connections to the optics were packaged in a sealed probe head. The probe had ST connectors which were interfaced to the spectrograph and the laser with short fiber-optic pigtails terminated with both an ST connector and an SMA-905 fiber-optic connector. The probe's optics coaxially aligned the laser and the detector optical fields and focused them about 1 cm from the probe head; the focussed spot diameter was less than 0.5 mm.

2.3.5 Fiber-Optic Filters

Optical filters, 3mm diameter and 0.5mm thick, were inserted between the finished ends of SMA-905 connectors. The filters were designed to reduce the fiber-optic silica Raman background and, as shown in Figure 2-3, were placed as close as possible to the probe head. For each laser source a different set of optical filters was required. The filter specifications and transmission characteristics for an argon-ion laser line (514.5nm) and a doubled Nd:YAG laser line (532nm) are shown in Appendix C.

The laser band-pass filter in the illumination fiber attenuates the silica Raman scattering generated in the illumination fiber but passes the laser line. In the collection fiber, a long-pass filter attenuates the laser light from the sample (and from other optical components) collected by the detector fiber. This filter reduces the silica Raman light produced in the collection fiber by the collected laser light.

2.4 Data Acquisition and Processing Software

Table 2-1 identifies the Raman data acquisition and data processing functions and the software used to perform those functions during the cold tests. Four different sets of software were used depending on the function being performed. (1) For spectrometer alignment, selection of binning parameters, and spectrometer/detector diagnostics, Princeton Instrument's *CSMA* software was used. (2) To obtain Raman spectra, Florida State University's (FSU) *RCAL/CCF*[1] data collection software was used. (3) FSU's *RCAL/ACHEM* package was primarily used for conversion of the collected data files to ASCII data files. (4) Finally, Galactic Industries' *GRAMS/386*[2] was used to read in the ASCII data files and perform the bulk of the data processing.

---

[1] *CSMA* is a registered trademark of Princeton Instruments

[2] *GRAMS/386* is a registered trademark of Galactic Industries

THIS PAGE INTENTIONALLY
LEFT BLANK

2.4.1 Spectrometer Set-up Software

Princeton Instruments, Inc., *CSMA* software was used to perform optical alignment and focussing of the spectrometer, selection of CCD detector binning parameters, and non-routine system trouble-shooting.

2.4.2 Data Acquisition Software

The FSU *RCAL/CCF* software records all raw spectra in binary format on the computer system's hard disk. The *CCF* package also performs an automatic dark-charge/white-light ("dark/white") correction of the raw data and stores, in addition to the original raw spectrum, the dark/white-corrected spectrum to disk. Spectral data files were then subsequently transferred to high-density floppy disks for further processing and archival operations. The FSU software automatically attaches a header to the spectral data file; this header contains selected system and sample information. To maintain traceability to the original raw spectral files during post-processing of the spectra, the FSU software copies the headers from the raw spectra to the post-processed spectral file headers. FSU post-processing software attaches new file name extensions to post-process spectra (1) to avoid over-writing and (2) to help maintain traceability to the original raw spectral files.

THIS PAGE INTENTIONALLY
LEFT BLANK

Table 2-1. Raman Data Acquisition/Processing Functions and Associated Software.

Function	Software Package (Vendor)

• Instrument set-up:
  • Perform optical alignment and focussing
  • Select binning parameters
• Maintenance, trouble-shooting
	CSMA v. 2.3A
	(Princeton Instruments, Inc).

• Real-time Raman data collection • Dark/white correction • Real-time spectral averaging • Create spectral file header	RCAL* / CCF v. 14 (Florida State University)
• Raman data post-processing • Data file format conversion	RCAL / ACHEM v. 14 (Florida State University)

• Raman data post-processing
  • Signal averaging
  • Silica Raman subtraction
  • Background correction
  • Spectral smoothing
  • Wavelength/wavenumber axis calibration
	GRAMS/386 v.3.0
	(Galactic Industries Corporation)

*Raman Chemical Analysis Library

2.4.3 Data Processing Software

GRAMS/386 was used for the bulk of the Raman data processing operations. These operations included:

(1) subtraction of silica background from sample spectra using either interactive or simplex subtraction methods,

(2) correction of non-Raman background features (e.g. fluorescence) using multi-point linear baseline corrections,

(3) smoothing operations using maximum likelihood techniques,

(4) wavelength calibration using a linear fit of peak wavelength value (in nm) *versus* peak pixel position from the associated neon wavelength reference spectra, and

(5) conversion of the resulting wavelength scale to Raman (Stokes) shift.

To convert from wavelength to Raman shift, wavelength values of 514.5309 nm for the argon-ion laser and 532.2 nm for the doubled Nd-YAG laser were used. The *GRAMS/386* package can provide data file audit-trail capability similar to that of the FSU software.

2.5 Software Issues

There are several software issues that remain to be addressed with respect to collecting, processing, and archiving Raman data. These issues include:

(1) automation of spectral data collection,
(2) automation of Raman spectral data processing,
(3) integration of Raman spectral data collection and processing functions,
(4) data archiving and retrieval capability, and
(5) verifying and validating the data collection, processing, and archiving/retrieval functions.

(1) Automation of Raman Spectral Data Collection: Collection of a Raman spectrum currently requires several discrete steps including collection of (a) dark-charge, (b) white-light, (c) wavelength-standard (e.g. neon lamp), (d) chemical-standard, and (e) sample spectra. These steps need to be automated to provide automatic collection of each spectrum as required. Automation will require the development of both control software and hardware (e.g. a fiber-optic multiplexer) to present to the spectrometer as needed the appropriate source (white light, wavelength standard, etc.).

(2) Automation of Raman Spectral Data Processing: Several Raman data processing steps are "labor-intensive" and will need to be automated prior to routine application of Raman spectroscopy to Hanford Site tank waste analysis. These are:

(a) probe-silica-Raman background subtraction,
(b) correction for other background features (e.g. luminescence),
(c) removal of "cosmic event" spikes in the spectrum (these were not an issue during the cold tests), and
(d) wavelength/wavenumber calibration of the spectral abscissa.

Calibration of the spectral intensity axis is an additional data-processing function that is currently unavailable and will require the development of Raman chemical standards, software, hardware, and data collection procedures.

(3) Integration of Raman Spectral Data Collection, Processing, and Archiving Functions: With the exception of the dark/white spectral data correction, most data collection, processing, and archiving functions are performed with separate software packages that use different file formats. Ultimately, a software system will be needed that smoothly integrates all these functions and uses a common file format.

3.0 GENERIC PROCEDURES

This section explains general procedures followed in acquiring Raman spectra.

3.1 Hardware Setup

The experimental work in this report used the basic equipment described above in Section 2.0. The steps described below were performed to set up the Raman system hardware.

3.1.1 Detector Setup

The detector dewar was filled with liquid nitrogen. The detector temperature controller was set at -120°C. The detector would reach this temperature in approximately two hours. If the detector could not reach this temperature, this usually meant that the detector vacuum was not sufficiently low (<20mTorr) and too much room heat was leaking into the detector. The detector would then be allowed to warm to room temperature before the detector dewar was connected to a vacuum pump to re-establish the proper vacuum level. The dewar needed to be pumped down about every two months to maintain proper evacuation.

3.1.2 Laser Startup

514.5-nm laser: After the power to the 514.5-nm laser was turned on, the laser was allowed to warm up for approximately one hour before testing. This allowed the laser output and the internal cabinet components to stabilize due to the thermal load imposed by the laser inside the cabinet.

532-nm laser: This laser system dissipated a smaller heat load than the 514.5-nm laser. After turning the system on, the unit would self-initialize and perform its fixed calibration routines. This procedure usually lasted five to ten minutes. However, there were occasions when calibration would extend beyond 15 to 20 minutes. When this happened, the automatic calibration would be interrupted. The laser controller was then connected to a computer and manual calibration would be performed via a software program.

3.1.3 Fiber-Optic Connections

Before connecting a probe to the Raman system, the SMA-905 feedthroughs on the fiber-optic bus panel and the fiber-optic connector ferrules were cleaned.

3.1.4 Probe Configuration

The probe was visually inspected to verify the configuration needed for testing and the probe serial number recorded. The distal end of the probe was cleaned by wiping the tip with isopropyl alcohol and allowed to air dry prior to testing.

3.1.5 Sample Preparation

When using the sodium nitrate or potassium chloride pellets, the samples would periodically be cleaned by wiping the surface with isopropyl alcohol and allowing the sample to air-dry. Occasionally, the pellets would generate a broad spectral feature after this process. In this case, the pellets would be placed in a 110°C oven for at least two days and their Raman spectra inspected for the absence of this broad feature prior to reuse as sample material.

Simulant material had a tendancy to experience layering effects if not used for a number of days. The simulant material was stirred to ensure a homogeneous mixture prior to use as sample material. Using standoff probes, a small amount of simulant (approximately one teaspoon) was placed on a sample tray (polyethylene disk). The probes were then positioned approximately 3mm from the sample tray. Mash probes allowed for the insertion of the probe directly into the simulant container. The probes were inserted approximately 1/4" into the sample material.

3.1.6 Probe/Sample Environment

To prevent exposure to room light, the distal probe end and sample were contained in a "light-tight" cardboard box. This prevented any spectral interferences from room lights in the collected spectra. All spectra were collected in this light-tight environment.

3.1.7 Spectrometer Settings

Spectrometer slit width, grating, and center wavelength settings would be initialized per testing requirements.

3.1.8 Computer/Software Settings

Directory: A directory was created for each testing campaign. The directory was labeled as YYMMDDX, where YYMMDD represents the Year, Month, and Day, and X is a sequential identifier (A, B, C, etc.).

RCAL: The FSU-developed RCAL program provided limited hardware setting documentation. Prior to its operation, the operator was required to input the following data which was automatically entered into the data file header:

- Operator Initials

- Date/Time
- Logbook Number/Page
- Laser Wavelength/Power
- Probe Type/Description
- Spectrometer Slit Width, Grating, and Center Wavelength

Logbook Setup: The logbook was prepared to document the test details including:

- Operator Name
- Test Date
- Probe Type
- Laser Wavelength/Power
- Spectrometer Slit Width, and Center Wavelength
- Detector Exposure Time/Coadds (number of spectra used to generate an averaged spectra)
- Filename and Comments

3.2 Wavelength Calibration

The spectrometer wavelength calibration was performed using a neon source as the wavelength standard. The neon lamp source provided strong emission lines in the 500-nm to 700-nm region over which most of the test data was collected over. The neon spectra were obtained using a 200-µm spectrometer slit width. A typical example of the spectrum from a neon line source is shown in Figure 3-1.

The wavelength calibration procedure then followed a three-step FSU-developed calibration process. These steps were implemented via the FSU-developed CLB.EXE program (Tseng, C.).

1) *Examination of Each Window*. Neon line spectra were recorded over the 540-nm to 660-nm region. For each window, a linear regression was calculated using the detector line position data and the known wavelengths of the neon lines. The linear regression then provides values for the center wavelength (λ_o) and dispersion (Ångstrom per pixel) for each spectral window.

2) *Dispersion vs. Wavelength*. A fourth-order polynomial was fitted to the Ångstrom-per-pixel values calculated for each window versus the center wavelength value for each window. The calculated coefficients were read by the data acquisition program to allow calculation of dispersion (Ångstrom per pixel) at any spectrometer setting.

3) *Pooling Pixel/Wavelength Data*. A quadratic equation was fitted to the pooled wavelength versus pixel number data from each window and the calculated coefficients were used in this final step to calculate the Raman shift for a specific point on a spectrum.

Figure 3-1. Neon Spectrum at 600nm Center Wavelength.

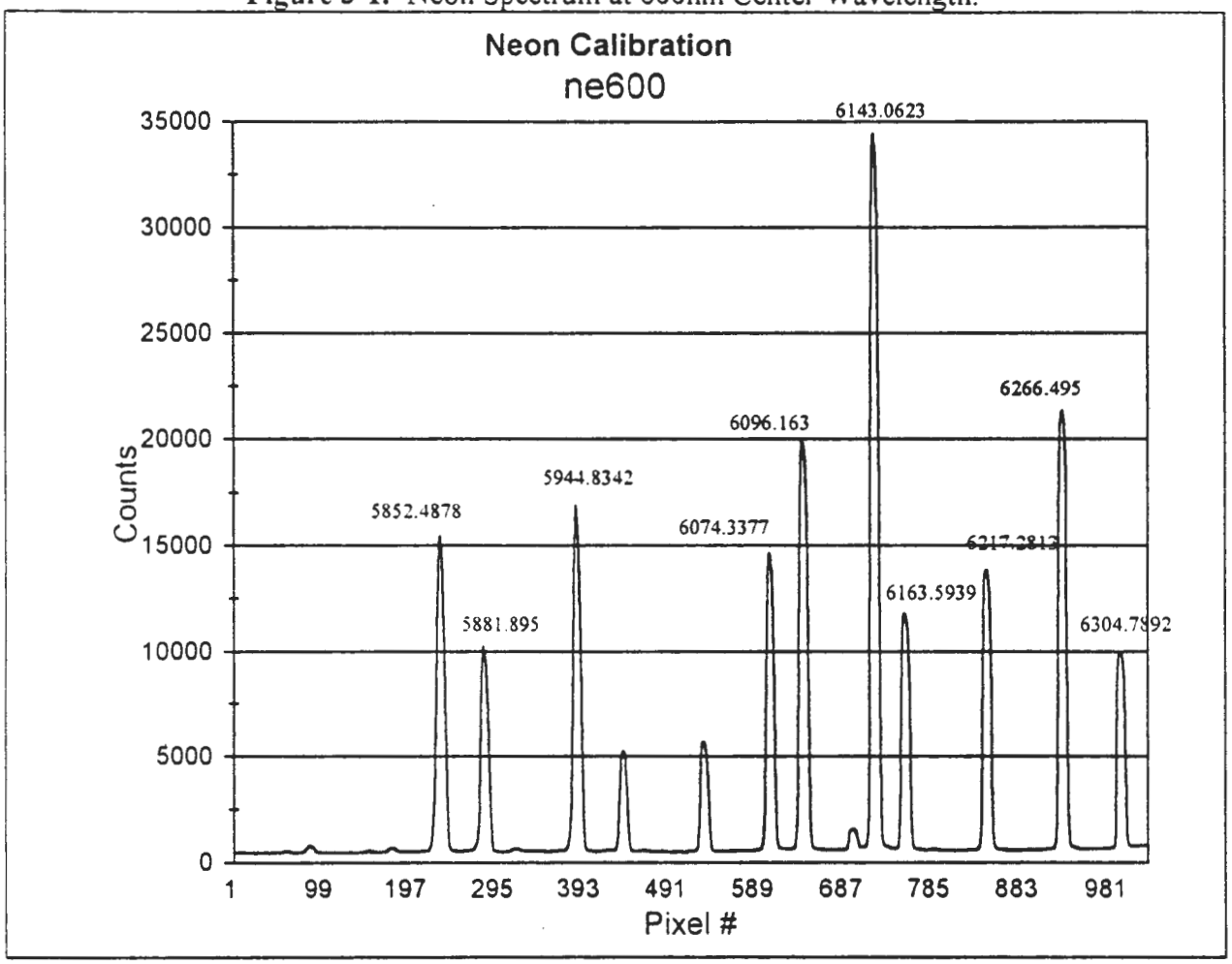

The quadratic equation corrects for slight non-linearities in dispersion across the face of the CCD detector.

For each spectral window, the CLB.EXE program requires that neon lines be properly identified. The individual calibration files were then combined and processed to form a single ASCII file containing all of the calibration parameters described above. As an example, the typical values for the LLNL system are shown in Table 3.1. Files with these values in it used the YYMMDD naming format with a .CLB extension. The FSU software requires that the file be placed in the RCAL directory where it can be read by the data acquisition program.

Table 3-1. Calibration Parameters, Typical Values.

Center Wavelength Slope	9.991689324378967e-01
Center Wavelength Intercept	2.552373123168945e+01
Lower Calibration Wavelength Limit	5.421036132812500e+03
Upper Calibration Wavelength Limit	6.620038574218750e+03
Å/Pixel C_0	5.956247234590497e-01
Å/Pixel C_1	8.826066331776199e-07
Å/Pixel C_2	-7.953684165425414e-09
Å/Pixel C_3	4.064912809919966e-12
Å/Pixel C_4	-1.148009991403049e-16
Lower Pixel Calibration Limit	2.371655273437500e+01
Upper Pixel Calibration Limit	9.931877441406250e+02
Pixel Position C_0	-4.889911902284261e+02
Pixel Position C_1	9.512783678079935e-01
Pixel Position C_2	-3.890107623763614e-06

3.3 Data Acquisition

In a typical Raman campaign several different types of spectra were recorded. As indicated above, each of the spectra have properties and features that are essential in extracting high-quality Raman information from spectra.

Table 3-2 lists the spectra typically collected during a Raman campaign and the requirements for each of the spectra (Douglas, J.G. 1994).

Table 3-2. Spectral Data Collected.

SPECTRUM TYPE	ACQUISITION ORDER	MAJOR PURPOSE/USE	SPECIAL ATTRIBUTES
neon	1*	(1) neon wavelength ref.	(1) record spectrum from a neon lamp * (2) record each time spectrometer grating position is moved
dark charge	2†	corrects for CCD dark charge contribution in all recorded spectra	(1) record with spectrometer entrance shuttered close (2) exposure time for dark spectrum must be the same as that of other spectra recorded † (3) record as often as needed to match sample spectra exposure times (4) must be first spectrum recorded when setting a new exposure time
white-light (tungsten lamp)	3	(1) correct for CCD pixel-pixel variation	(1) record spectrum of tungsten lamp (2) must have good S/N - total integration time must be, at a minimum, equal to total integration time of longest anticipated sample integration time; typical integration times are 0.5 - 2 minutes
probe response	4	correct the probe's silica Raman spectrum, spectrum for silica probe Raman response	(1) record spectrum using Raman inactive material (e.g. KCl) (2) must have good S/N - total integration time must be at minimum equal to total integration time of longest anticipated sample integration time; typical integration times are 0.5 - 2 minutes
samples	5	record Raman spectra from samples	(1) Exposure times must match that of the dark spectrum. (2) White-light spectra must be taken with same system setup/operational parameters. (3) Pixel count levels for spectra should be in the upper 3/4 of the detector range.
neon	6	final wavelength calibration check/verification	

4.0 RAMAN DATA

This section summarizes the key tests performed during FY 1994. Section 4.1 begins with a description of the chemical standards used to acquire signal-to-noise, silica response, and probe efficiency data. Section 4.2 describes the process used to calculate signal-to-noise values. Section 4.3 tabulates fiber-optic probe performance based on signal-to-noise, silica response, and probe efficiency. Finally, Section 4.4 presents the results of the Raman interrogation of tank waste simulants.

4.1 Chemical Standards

Three areas were evaluated in measuring probe performance: signal-to-noise ratio, probe silica response, and probe efficiency (see Section 4.3). Sodium nitrate and potassium chloride were used as the standards for measuring the signal-to-noise ratio and probe silica response, respectively. These were chosen for the following attributes:

(1) chemical stability (with respect to time, exposure to laser radiation, and exposure to ionizing radiation),
(2) potassium chloride exhibits no Raman activity; this allows only the probe's Raman response to be measured,
(3) sodium nitrate yields sufficiently intense Raman bands appearing within the desired spectral window,
(4) ease of handling,
(5) low toxicity, and
(6) low chemical hazard.

Sodium nitrate is a translucent material that shows little or no absorption of light in the wavelength region of 500 to 600 nm. This is in contrast to the simulant material that completely absorbs the laser light, preventing any light from escaping outside the sample chamber. The concern here is that the signal-to-noise measurements were made on a material that does not closely mimic the tank waste. Hence, the S/N measurements, though adequate in comparing probes combined with other factors, are not made with standards that closely mimic high-level waste simulants and samples.

During the initial stages of testing, a comparison was made between sodium nitrate in a powdered form to a compressed pellet of sodium nitrate. The purpose of the test was to investigate the signal reproducibility of the sample material. The relative standard deviations (RSD) of the

corrected peak height[1] of the sodium nitrate Raman band at 1067.5 cm^{-1} as measured for granular and pelletized forms of sodium nitrate were calculated. The granular sodium nitrate was used as received from the vendor. Nitrate pellets were formed by finely powdering approximately 10 grams of sodium nitrate in a ball mill, then compressing the powder in a hydraulic press. For each of the two sample forms, spectra were collected at three different points in the samples using the WSRC chisel-tip probe. For the granular form, the RSD was 0.133; for the pellet form the RSD was 0.023. Because the RSD of the pelletized form appeared superior to that of the granular form, the more easily handled pellets were used for subsequent testing.

4.2 Signal-to-Noise Measurements

4.2.1 S/N Processing

This section describes the process used to calculate signal-to-noise ratios that result from relatively high frequency noise within a Raman spectrum. In contrast to silica Raman noise, this noise is high frequency and includes noise from electronic sources, pixel to pixel detector variations, optically induced detector noise, etc. This noise is the fundamental limiter in extracting low level Raman signals from a Raman spectrum. The signal-to-noise ratio was a parameter used in evaluating a probe's performance (See Section 4.3). A solid pellet of sodium nitrate was used as the sample material for all S/N determinations.

The signal-to-noise ratio was calculated from dark-charge, white-light, probe-silica corrected spectra (see Appendix B) and is defined as:

$$(S/N)_{\Delta\nu} = \frac{I_{\Delta\nu}}{sd_B}$$

---

[1] Relative standard deviation of the corrected peak height is given as:

$$RSD_h = \frac{std.\ dev.\ of\ the\ corrected\ peak\ height}{average\ corrected\ peak\ height}$$

where the corrected peak height is given as:

$$corrected\ peak\ height = counts\ at\ peak\ maximum - background\ counts$$

Figure 4-1. Typical Regions of Sodium Nitrate Spectrum Used for S/N Calculations.

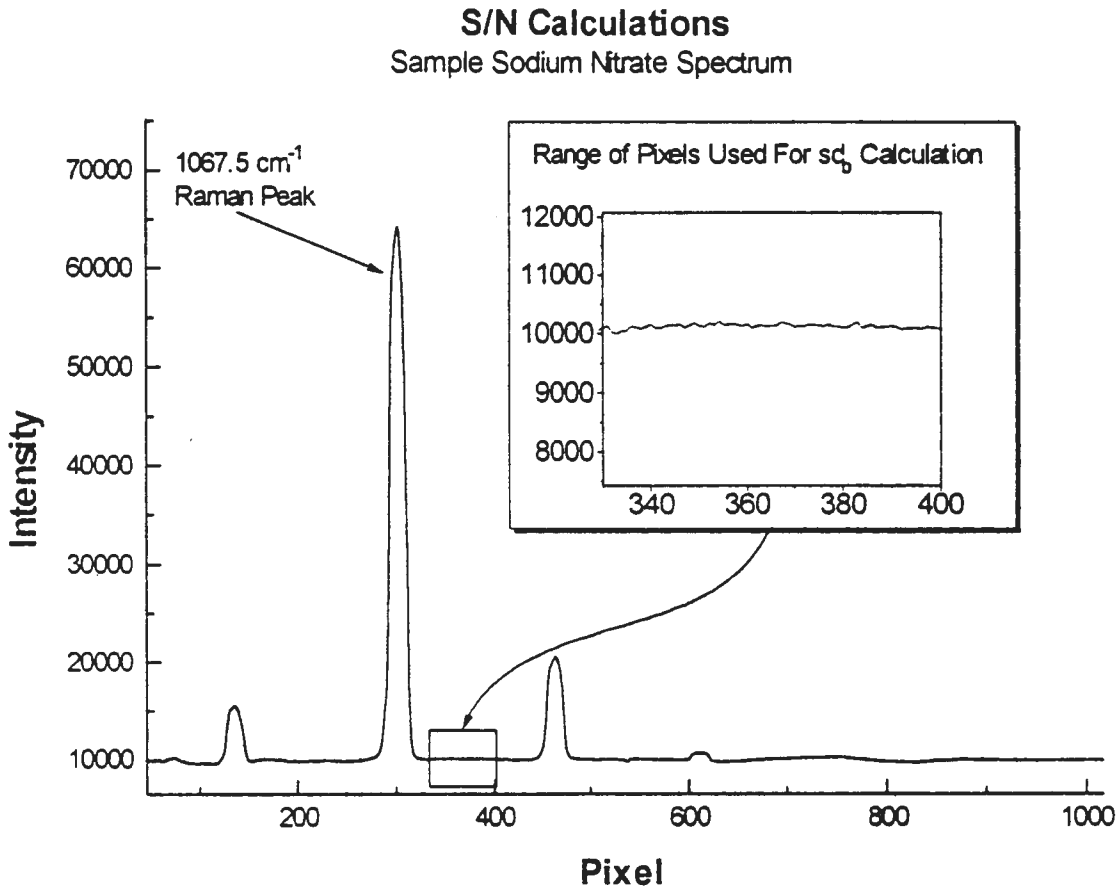

where $(S/N)_{\Delta\tilde{\nu}}$ is the signal-to-noise ratio for a Raman peak located at some Stokes shift $\Delta\tilde{\nu}$, $I_{\Delta\tilde{\nu}}$ is the baseline-corrected peak intensity for the peak at $\Delta\tilde{\nu}$ from the true spectrum, and sd_B is the standard deviation of the random noise measured on the baseline in the vicinity of the Raman peak at $\Delta\tilde{\nu}$, also from the true spectrum.

In the work reported here, all S/N calculations were performed using the 1067.5 cm^{-1} sodium nitrate peak. An average background value (used to correct the peak height) and sd_B were calculated using 60 background points located to the right of the nitrate peak as shown in Figure 4-1.

In general, the Raman S/N calculations were performed using the following experimental conditions:

Excitation Wavelength:	532 nm (514.5 nm for the EIC probe)

Spectrometer Center Wavelength:	555 nm
Spectrometer Slit Width:	200 μm
Sample:	Sodium Nitrate Pellet

4.2.2 System Repeatability and Sample Repeatability S/N Measurements

Additional tests were performed to determine the impact of the system and sample on the repeatability of the signal-to-noise calculations. The purpose of these tests was to determine the potential impact of the Raman hardware and the physical and optical properties of the sample on S/N measurement repeatability.

In these tests, ten spectra of a sodium nitrate pellet were taken:

1) keeping the probe position constant (System Repeatability) and
2) repositioning the probe to different points on the sample (Sample Repeatability).

Specific experimental conditions were:

Probe:	WSRC S2-002 Thin Window With Filters[2]
Laser:	135.3mW @ 514.5nm
Slit Width:	200μm
Center Wavelength:	555nm
Total Integration Time:	30s

Signal-to-noise values were calculated for each spectrum and the standard deviation computed for each set of signal-to-noise values. The standard deviation of the S/N values for system repeatability and sample repeatability were 128 and 101, respectively. A two-tailed F test at the 95% probability level shows these two standard deviations are not significantly different. Therefore, these results show that the sodium nitrate pellet is sufficiently homogeneous to not warrant an accurate replication of the probe position on the pellet each time a measurement is made. These results provided a reasonable determination of the measurement repeatability for future reference.

---

[2] Laser Band-Pass Filter:
Manufacturer: CVI, Coating: FO6-514.5-3mm

Long-Wave-Pass Filter:
Manufacturer: CVI, Coating: LWP-523-3mm-WH

Transmission data discussed in Section 5.4.

4.3 Probe Comparison Tests

4.3.1 Purpose

In the evaluation of the Raman system, a number of basic performance issues were found to be related to the type of Raman probe being used. Originally, probe tests were performed to identify probes with superior S/N ratios. Spectral signal-to-noise ratios are important because they determine the detection limits for molecular species in samples. As discussed in Section 4.2, the S/N values for probe comparisons were determined using sodium nitrate spectra. However, as Raman data were acquired from real tank wastes and from simulant materials, other probe performance parameters were identified as important issues. During the course of the testing campaigns, two other factors, probe silica response and probe efficiency, were considered.

Silica response is the Raman response from the silica fiber-optics. As a comparison factor, silica response is calculated as the ratio of an arbitrary silica peak to an arbitrary Raman peak:

$$Silica\ \ Response = \frac{Raman\ \ peak\ \ height\ - Baseline}{Silica\ \ peak\ \ height\ - Baseline}$$

where *Baseline* is defined as the average count level taken on either side of the peak. For the data shown below, the 724-cm^{-1} Raman peak and the 803-cm^{-1} silica peak using sodium nitrate spectra were used. An example of these peak locations and resulting silica response ratio is shown in Figure 4-2.

The Raman signal is also a function of the laser power delivered to the sample and the integration time of the detector. Probe efficiency uses these two variables to "normalize" the probe response. The result is a sensitivity figure of merit that is independent of these other system parameters. Fiber-optic probe efficiency was calculated as:

$$Probe\ \ Efficiency = \frac{Raman\ \ peak\ \ height\ - Baseline}{laser\ \ power\ \times\ exposure\ \ time}$$

where the laser power was measured at the distal end of the probe and the 1067.5 cm^{-1} sodium nitrate Raman peak was used for these calculations. For both the silica response and probe efficiency calculations, the raw dark-charge/white-light corrected files were used without any probe silica corrections.

Figure 4-2. Example Spectrum for Calculating Silica Response Factor.

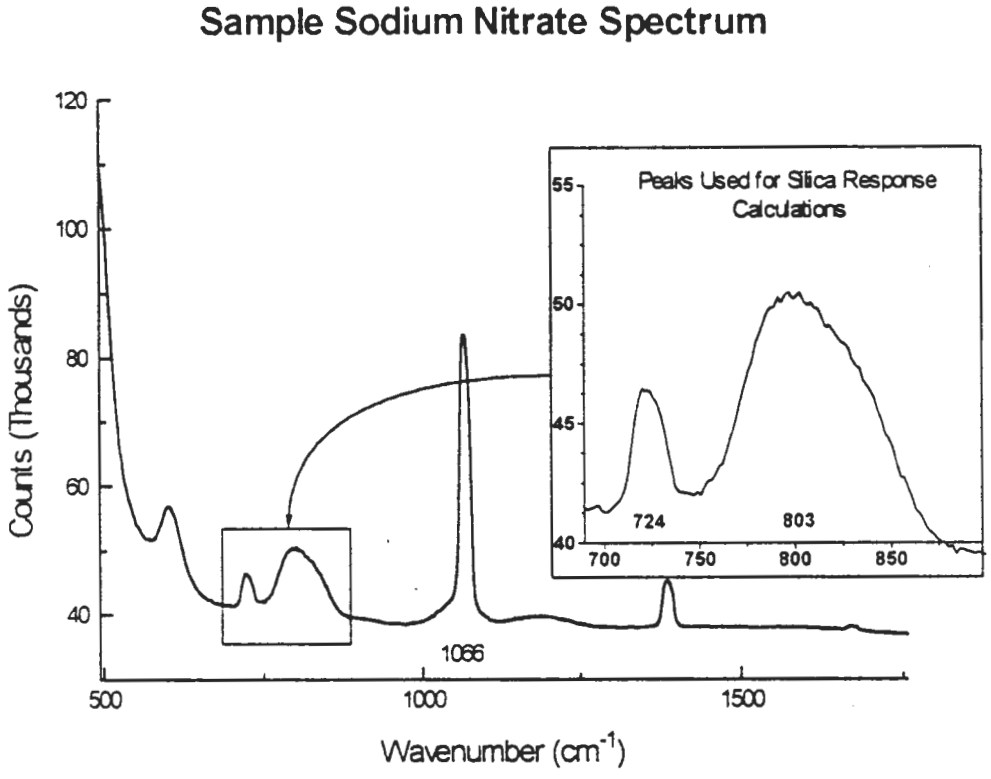

4.3.2 Comparison Data

Figure 4-3 provides a spectral comparison of sodium nitrate for each probe tested. The 514.5nm and 532nm excitation wavelengths are sufficiently close to allow direct comparison of the probes. Optical filters (see Appendix C for a description of the filters) were used in both the laser and receiving fibers for the Polytec and WSRC probes. Table 4-1 summarizes the probe performance data. Probes with superior performance factors are highlighted. Both the WSRC chisel-tip probe and the 36-around-one flat-face probe exhibited some background luminescence that probably reduced the signal-to-noise values for these probes.

Three factors that should be considered when selecting a fiber-optic probe design for remote Raman spectroscopy were identified: (1) signal-to-noise ratio, (2) the intensity of the probe's silica Raman spectrum, and (3) the probe's efficiency. Of the five probes tested, the following conclusions were made:

(1) The flat-face probes are most efficient at getting light to the spectrometer as measured by the efficiency factor. These probes use no optical filters.

(2) The NIR diffuse-reflectance probe is least efficient, but has superior S/N and silica peak ratio values.

Figure 4-3. Probe Comparison of Dark-Charge/White-Light Corrected Sodium Nitrate Spectra.

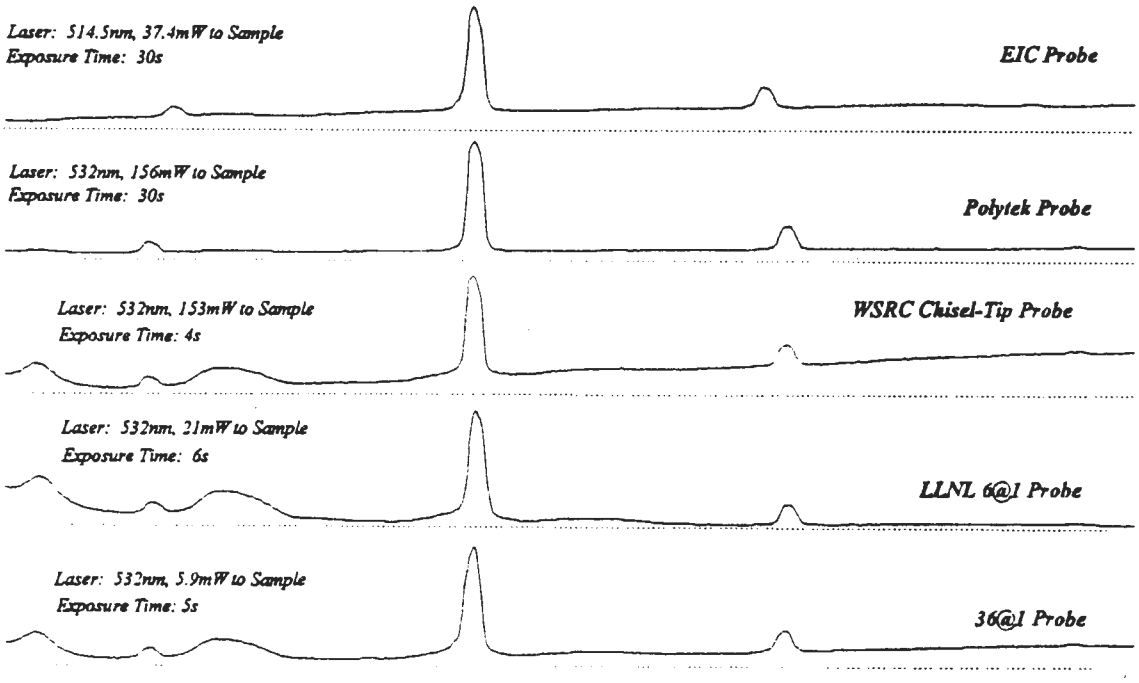

(3) The flat-face probes and the chisel-tip probe have a significantly higher silica response than do the NIR diffuse-reflectance and co-axial probes.

As discussed in Section 4.1, the sodium nitrate pellet target used to measure S/N may not have been the most appropriate due to its translucent features. Work should be done to explore a suitable standard that more closely mimics the optical characteristics of the tank waste.

Table 4-1. Comparison Summary.

Probe	Experimental Conditions			Comparison Factors		
	Laser (nm)	Power Delivered (mW)	Exposure Time (s)	S/N	Silica Peak Ratio	Efficiency (C/Ws)
EIC Co-Axial	514.5	37.4	30	897	2.75	38,300
Polytek NIR Diffuse Reflectance	532	156	30	1,635	4.40	12,000
WSRC Chisel Tip	532	153	4	435	0.5	46,900
LLNL Flat Face 6 Around 1	532	21	6	928	0.43	373,000
Flat Face 36 Around 1	532	5.9	5	208	0.61	1,630,000

4.4 Tank Waste Simulant Spectra

This section summarizes the diffuse-reflectance and Raman spectra obtained from four tank waste simulants: BY-104 saltcake, SY-101 sludge, T-Plant top sludge, and T-Plant bottom sludge. These spectra were collected to:

(1) determine how well the various probe types and laser excitation wavelengths would perform with materials similar to those of real tank wastes,
(2) determine the spectral absorption characteristics of tank-waste-like materials, and
(3) determine what species could be detected in these materials.

The rest of this section contains a description and results of (1) simulant diffuse-reflectance (optical absorption) studies, and (2) the Raman spectra obtained from the simulants; each section ends with the conclusions derived from these tests. Descriptions and the chemical compositions of the four tank waste simulants examined in this study are given in Appendix E.

4.4.1 Tank Waste Simulant Diffuse-Reflectance Studies

Figure 4-4 shows the resulting diffuse-reflectance spectra for each simulant. Experimental conditions for spectral data collection are summarized in Table 4-2.

To collect the diffuse-reflectance spectra, the same instrumentation as that used to collect Raman spectra was used with a tungsten-halogen light source substituted for the laser. The output of the tungsten-halogen source was coupled to the central fiber of a 36-around-one fiber-optic probe. The sample was illuminated with the probe set at 45° to the normal to the sample surface to minimize specular reflectance from the sample surface; the probe tip was approximately 7mm from the viewing point on the sample surface. The surrounding 36 fibers of the probe collected the non-absorbed, diffusely scattered light from the sample surface and returned the light to the monochromator. The monochromator's 300-g/mm grating was used as the dispersive element.

For each simulant, spectra were collected from 325 to 1100 nm in seven overlapping spectral windows. With each simulant spectrum, a white-light reference spectrum was also collected using a proprietary polymer target with a reasonably flat spectral response across the spectral region surveyed. All reflectance spectra were corrected for CCD detector dark charge. Each simulant diffuse-reflectance spectrum was ratioed to its corresponding dark-charge-corrected white-light spectrum to generate a relative reflectance spectrum. For each simulant, a composite spectrum over the complete spectral range was generated by splicing together the overlapping portions of the seven spectral windows. Finally, the wavelength axis was calibrated based upon a linear fit of center wavelength position of the spectrometer to the center pixel value in each spectral window. No scattering corrections were applied to the spectra.

Figure 4-4 shows that, in general, the simulants have a maximum absorbance at about 425 nm with absorbance tending to decrease toward longer wavelengths. The BY-104 simulant spectrum (trace A) shows an almost monotonic decrease in absorbance out to about 1000 nm while the SY-101 simulant spectrum (trace B) exhibits an absorbance minimum at about 900 nm. The T-Plant bottom spectrum (trace C) exhibits a plateau in its absorbance minimum extending from about 760 to 1000 nm; the T-Plant top spectrum (trace D) shows a distinct absorbance minimum at about 760 nm.

The important conclusion from these spectra is that laser light with wavelengths in the 400- to 600-nm range will be more efficiently absorbed by these samples than laser light emitted at longer wavelengths. Therefore lasers with longer wavelengths may be better excitation sources for these

Figure 4-4. Tank Waste Simulant Diffuse-Reflectance Spectra: (A) BY-104, (B) SY-101, (C) T-Plant Bottom, (D) T-Plant Top.

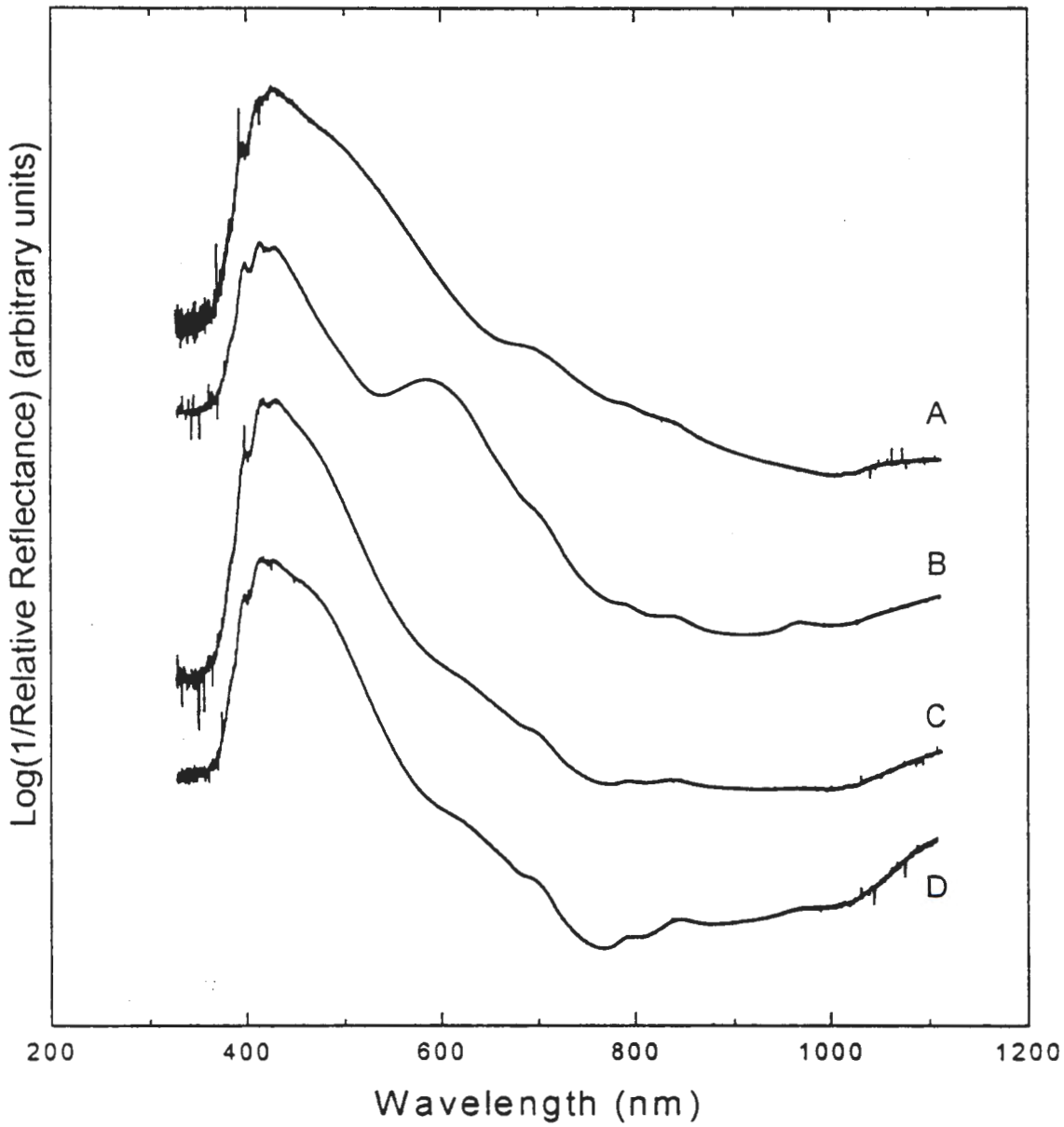

samples (and possibly for actual tank waste samples) because (1) more excitation photons will presumably be available to stimulate Raman scattering and (2) the sample will absorb fewer of the longer-wavelength, Stokes-shifted photons. However, since Raman scattering efficiency is proportional to the fourth power of the excitation frequency, longer-wavelength lasers will not

stimulate Raman scattering as efficiently as shorter-wavelength lasers. Further tests with longer-wavelength lasers using waste simulants and actual waste samples will be required to determine if the trade-offs among a number of system factors will generate a net increase in the Raman signal-to-noise ratio with longer-wavelength excitation. System factors that may improve the signal-to-noise ratio are (1) reduced sample absorbance, (2) reduced sample luminescence (possibly), and (3) increased transparency of the silica fibers. Factors working against a better signal-to-noise ratio at longer wavelengths include (1) poorer Raman scattering efficiency and (2) lower silicon-CCD-detector quantum efficiency.

Table 4-2. Experimental Conditions for Simulant Diffuse-Reflectance Spectra.

Parameter	Setting
Probe	36-around-1 probe; central fiber used to illuminate sample, surrounding fibers used to capture diffuse reflectance
Probe/sample geometry	probe at 45° from normal to sample surface; probe 7 mm from viewing point on sample surface
White-light source	tungsten-halogen lamp
White-light reference	proprietary white polymer
Spectrometer slit width	400 μm
Spectrometer slit height	15 mm
Grating	300 g/mm
Spectral window center wavelengths	450, 540, 630, 720, 810, 900, 990 nm
Single spectrum total acquisition time	1 min/window

4.4.2 Tank Waste Simulant Raman Spectra

Appendix B discusses the data treatment used to produce the Raman spectra shown in this section. As a general note, the simulants tested exhibited little or no luminescence; therefore, most of the simulant spectra shown in this section did not require any background correction for luminescence features.

Figure 4-5. Raman Spectrum of BY-104 Simulant: Oxyanion Region.

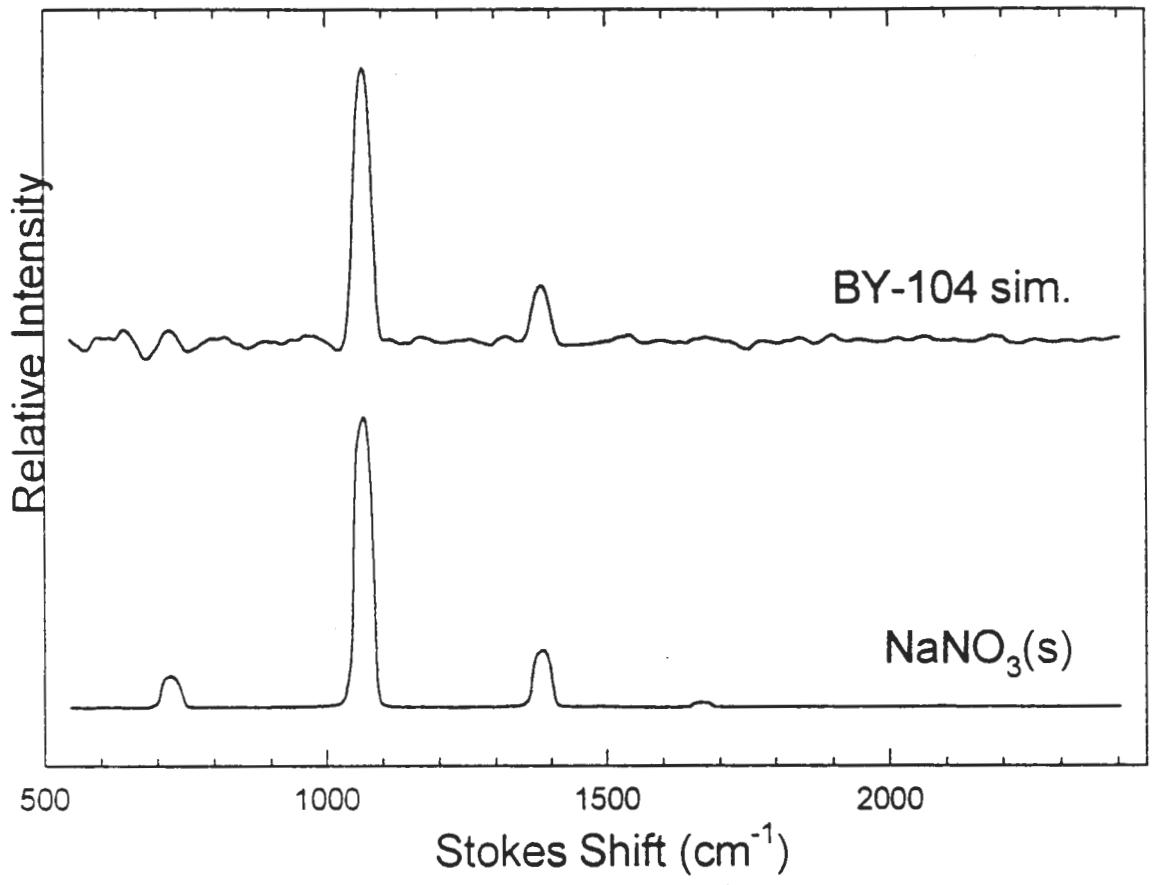

BY-104 Saltcake Simulant: Figure 4-5 shows the Raman spectrum collected for this simulant in the oxyanion spectral region. The major features of this spectrum are due to sodium nitrate which is the primary component of this material; no identifiable Raman features were visible at higher wavenumbers. These spectra were obtained with the Polytec PI, Inc., diffuse-reflectance probe equipped with laser band-pass and long-pass filters (see Appendix C); the excitation frequency was 514.5 nm. Peak positions (cm^{-1}) for the major peaks in the BY-104 simulant spectrum are 722.1, 1065.4, and 1383.2; measured peak positions for the sodium nitrate (solid) sample run during the same session are 723.9, 1066.6, and 1384.3.

SY-101 Convective-Layer Simulant: Figures 4-6 and 4-7 are the Raman spectra for the SY-101 simulant; Figure 4-6 compares the simulant spectrum of the oxyanion region with that of an actual SY-101, Window-E, convective-layer tank waste sample. Table 4-3 lists the prominent peak positions and likely identities of the compounds generating the peaks. These spectra show that

major waste components such as sodium nitrate and sodium nitrite are easily visible in this waste matrix. Furthermore, for the SY-101 simulant, the chelating agent ethylenediamine tetraacetic acid, tetrasodium salt ($Na_4EDTA \cdot 2H_2O$) is easily detected at the 5.5 weight % level. No identifiable Raman peaks were visible in the CH-stretch region for the actual SY-101 tank waste.

The spectra of the simulants were taken with 532.2-nm excitation using a WSRC chisel-tip probe with both laser band-pass and long-pass filters. The spectrum of the Window-E SY-101 tank waste was acquired with 514.5-nm excitation using a probe identical to that used for the simulant. The oxyanion-region spectra were smoothed using maximum likelihood smoothing; the spectrum of the SY-101 simulant in the CH-stretch region was not smoothed prior to plotting.

Figure 4-6. Raman Spectra of SY-101 Simulant and SY-101 Tank Waste: Oxyanion Region.

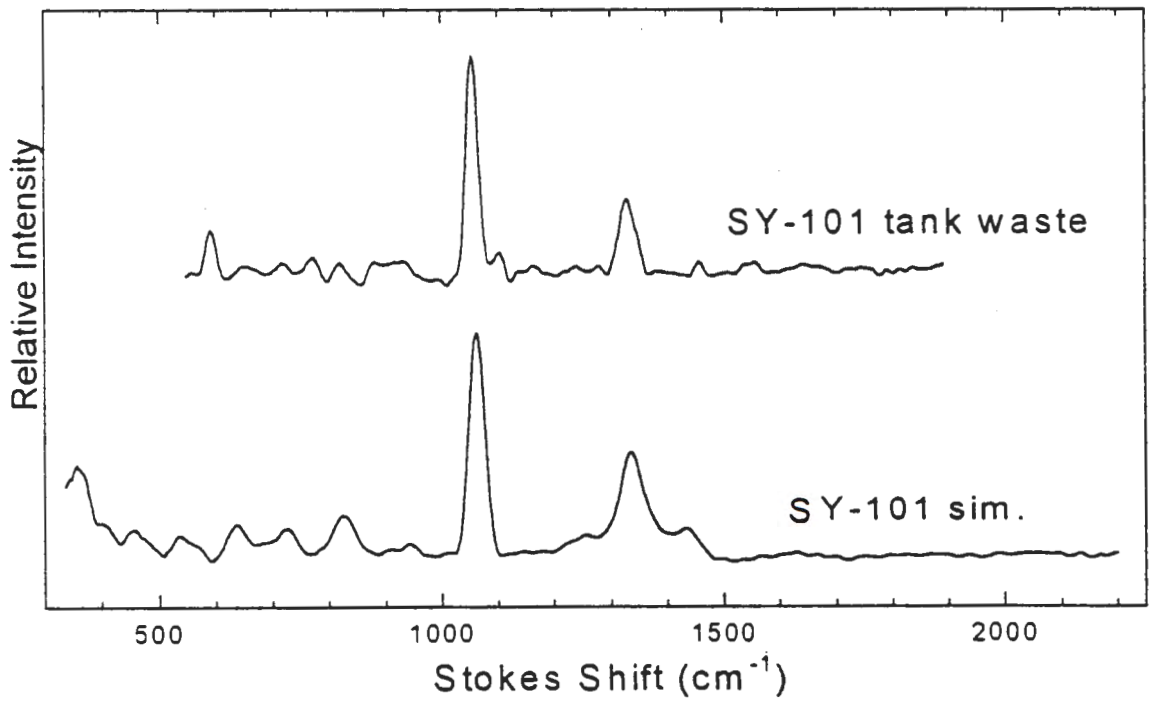

Figure 4-7 Raman Spectra of SY-101 Simulant and SY-101 Tank Waste: Ferrocyanide/CH-Stretch Region

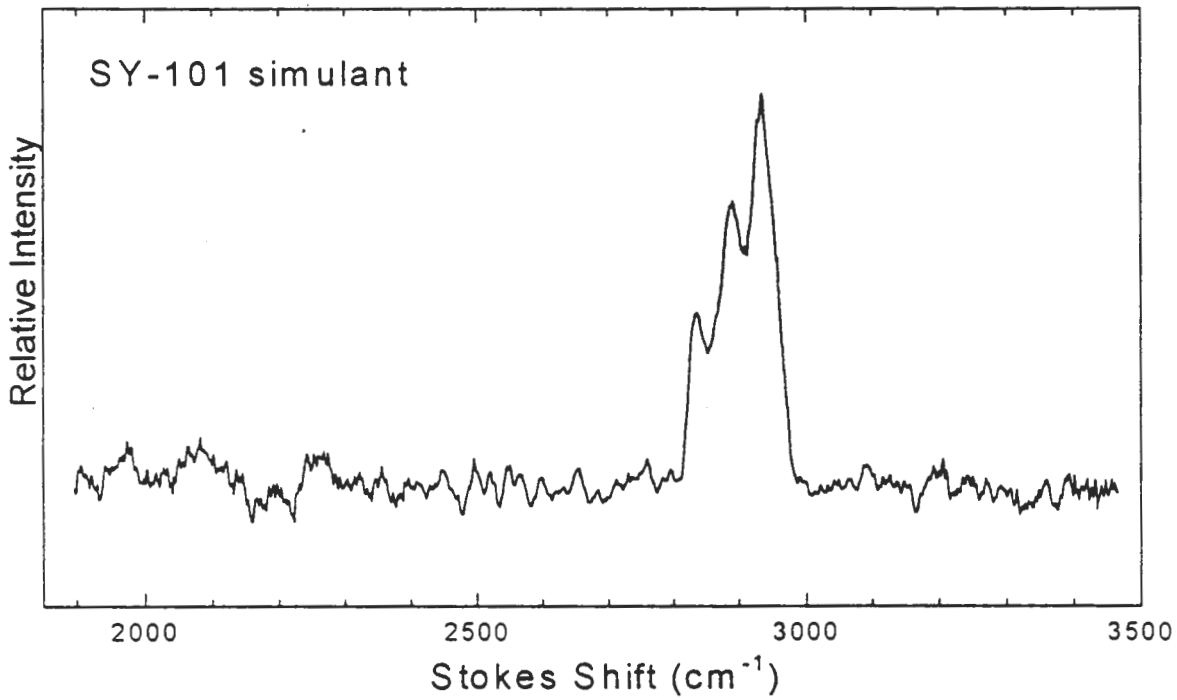

Table 4-3. Prominent peaks found in SY-101 simulant and tank waste and Raman spectra.

Line Position (cm^{-1})	Probable Compound	Approximate Concentration (wt%)
SY-101 Window E sample		
590.7	residual probe silica(?)	---
717.4, 1053.9	saturated aq. $NaNO_3$	12
772.3	unknown	---
818.3, 1328	saturated aq. $NaNO_2$	20

Line Position (cm^{-1})	Probable Compound	Approximate Concentration (wt%)
1104	unknown	---
1457	unknown (sodium oxalate?)	---
SY-101 Simulant		
718.7, 1054.9	saturated aq. $NaNO_3$	13.4
816.9, 1328.4	saturated aq. $NaNO_2$	16.2
934.8, 1424.6, 2836.7, 2885.7, 2937.2	$Na_4EDTA \cdot 2H_2O$	5.5

T-Plant Top Simulant: Figures 4-8 and 4-9 show spectra obtained for this simulant in the oxyanion and CH-stretch regions. Prominent peaks in these spectra are 826.2 (unknown), 1051.5 (aqueous nitrate), and 2103.9/2139.7 (sodium nickel ferrocyanide) cm^{-1}. The spectra of sodium nitrate (major peaks at 725.6, 1067.5, and 1386 cm^{-1}) and sodium nickel ferrocyanide (major peaks at 2102.4 and 2138.6 cm^{-1}) are included for reference. The T-Plant top simulant spectra in Figures 4-8 and 4-9 were obtained with 532.2-nm excitation. The Polytec PI, Inc., diffuse-reflectance probe was used with laser band-pass and long-pass filters to obtain the data in Figure 4-8 and the WSRC chisel-tip probe with band-pass and long-pass filters for the data in Figure 4-9. For this material, the diffuse-reflectance probe generated less Raman silica background than did the WSRC probe; the reduced probe-silica background greatly simplified removal of the probe-silica background. The sodium nickel ferrocyanide spectrum in Figure 4-9 was generated using a different Raman instrument with 514.5-nm excitation.

Figure 4-8. Raman Spectrum of T-Plant Top Simulant: Oxyanion Region.

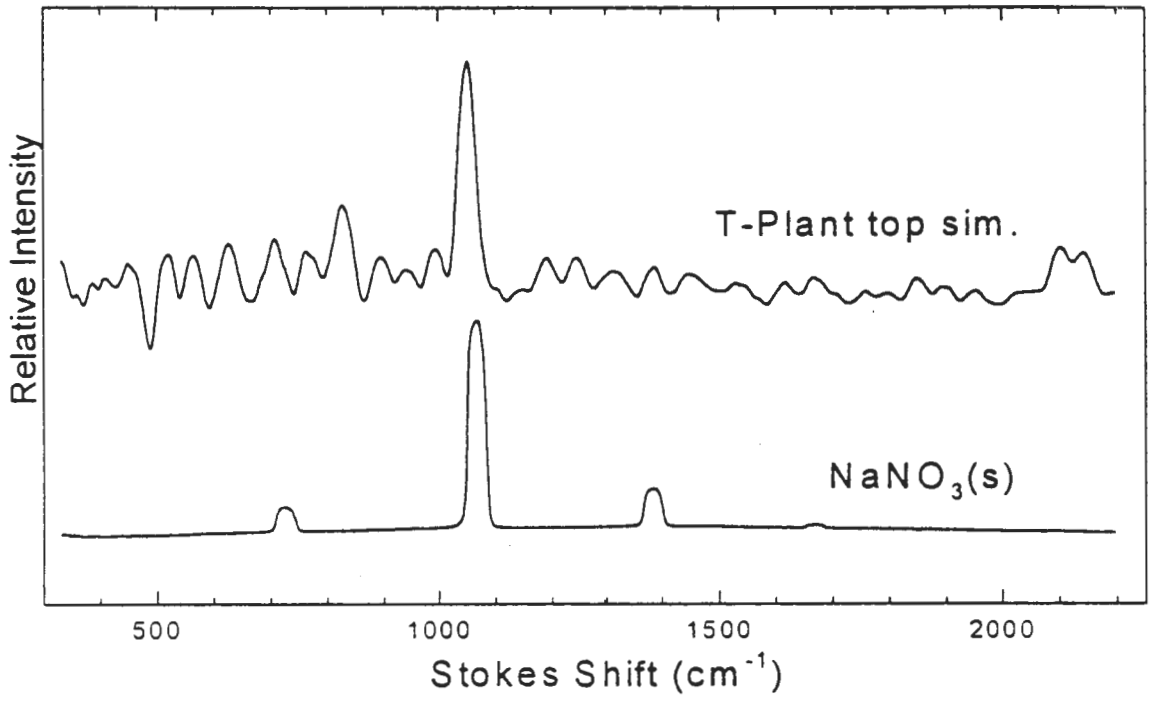

Figure 4-9. Raman Spectrum of T-Plant Top Simulant: Ferrocyanide and CH-Stretch Regions.

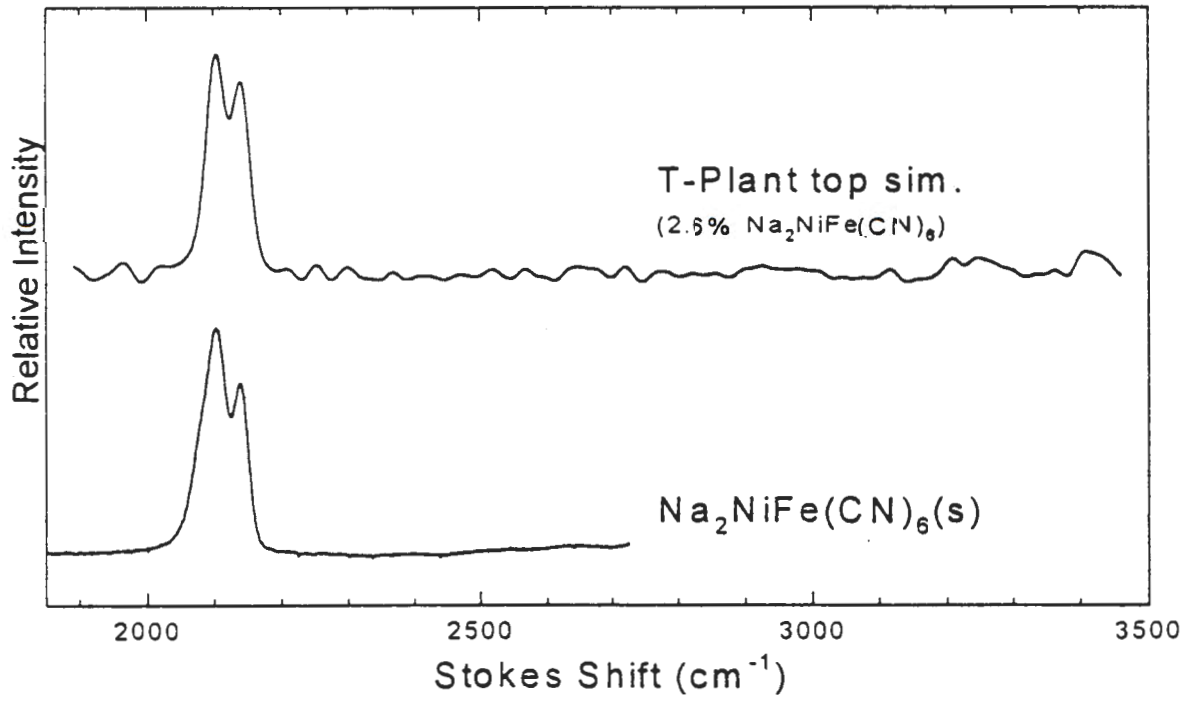

Figure 4-10. Raman Spectrum of T-Plant Bottom Simulant: Oxyanion Region.

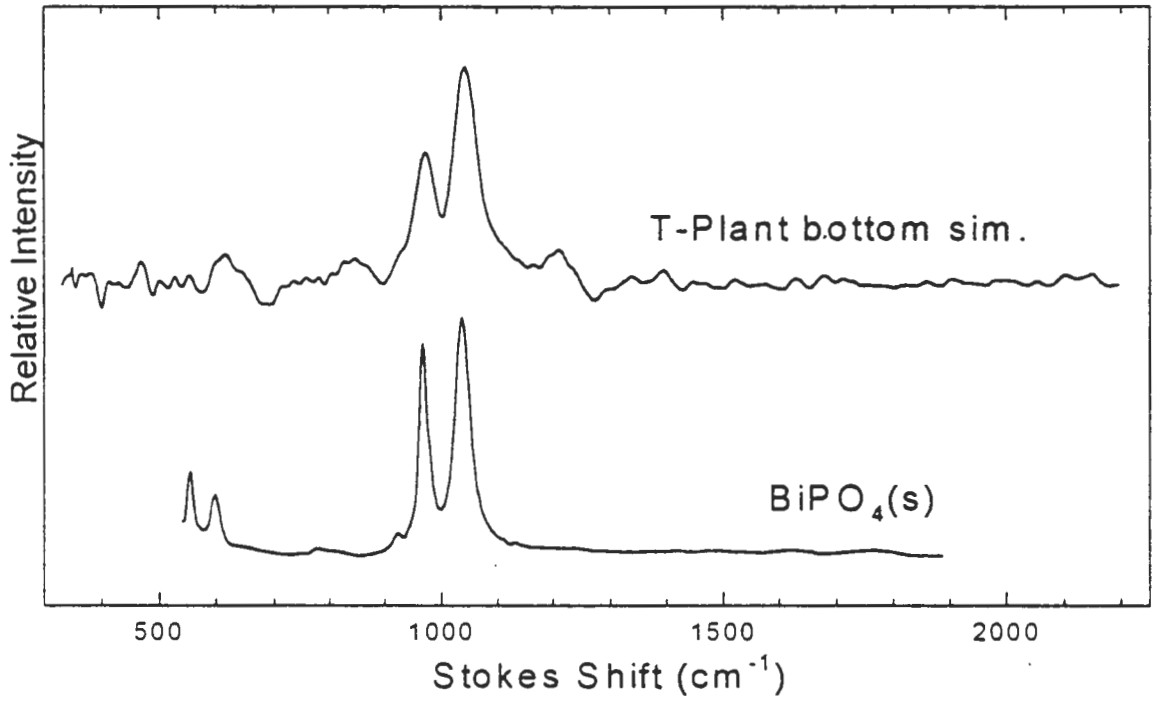

T-Plant Bottom Simulant: Figures 4-10 and 4-11 show spectra obtained for this simulant in the oxyanion and CH-stretch regions. Prominent peaks in these spectra are 972.2/1041.9, and 2101.3/2141.1 cm^{-1}. The spectra of bismuth phosphate (solid; major peaks at 966.9 and 1036.2 cm^{-1}) and sodium nickel ferrocyanide (solid; major peaks at 2102.4 and 2138.6 cm^{-1}) are included for reference. The primary feature to note is that, for this simulant with a sodium nickel ferrocyanide content of only 0.84 weight%, the signal-to-noise ratio is sufficiently good to clearly define the ferrocyanide signal in the spectrum.

The T-Plant bottom simulant spectra in Figures 4-10 and 4-11 were obtained with 532.2-nm excitation. The diffuse-reflectance probe was used with laser band-pass and long-pass filters to obtain the data in Figure 4-9 and the 36-around-one probe to obtain the data in Figure 4-11. As with the T-Plant top simulant, the low probe-silica background of the filtered diffuse-reflectance probe simplified removal of the probe-silica background. Of all the probes used to collect spectra of this simulant in the CH-stretch region, the 36-around-one probe provided the best signal-to-noise ratio for the ferrocyanide peaks.

Additional examination of the two spectra in Figure 4-10 reveals that the bismuth phosphate peaks in the T-Plant bottom spectrum appear red-shifted and broader than the peaks of the dry bismuth phosphate sample. These differences may be due to:

Figure 4-11. Raman Spectrum of T-Plant Bottom Simulant: Ferrocyanide and CH-Stretch Regions.

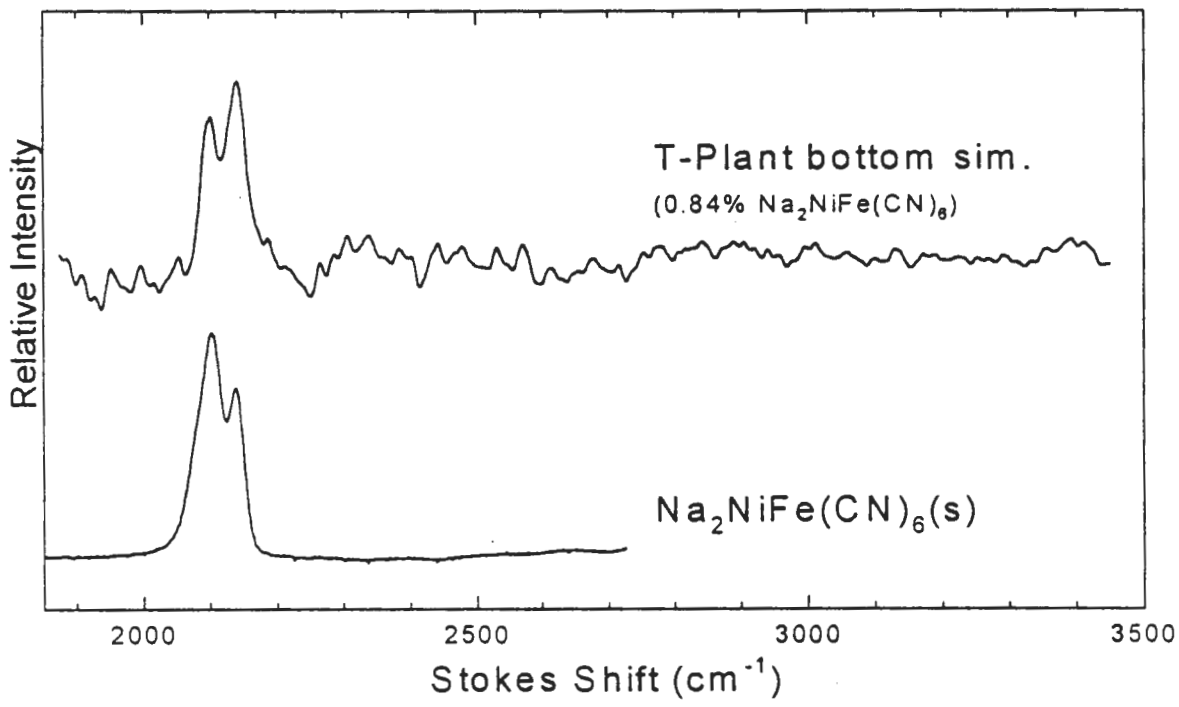

(1) hydration of the bismuth phosphate in the T-Plant bottom simulant,
(2) differing instrument resolutions (the bismuth phosphate reference spectrum was aquired using a different instrument at higher resolution), and
(3) convolution of the T-Plant bottom bismuth phosphate signal with that of nitrate.

In Figure 4-11, the differences between the two ferrocyanide spectral bands may be due to (1) the poorer signal-to-noise ratio of the simulant spectrum compared to the reference spectrum and/or (2) real chemical differences between the ferrocyanide species generating the signals.

Conclusions from Tank Waste Simulant Spectra:

(1) For the T-Plant simulants, the presence of sodium nickel ferrocyanide species is detectable at least as low as 0.84 weight%.
(2) In the oxyanion region, probes with low-silica-Raman backgrounds, such as the diffuse-reflectance probe with filters, produced the spectra most readily treated to remove the silica-Raman background signal. Adequate filtering of the probe silica-Raman background is important for at least two reasons:
    (a) to reduce spectral shot noise caused by large silica-Raman backgrounds and

(b) to avoid spectral artifacts generated during the spectral subtraction of the silica-Raman background.

(3) In the ferrocyanide and CH-stretch regions the probe silica-Raman background is not as significant as it is in the oxyanion region. Therefore, those probes most capable of collecting large amounts of the scattered Raman signal, such as the 36-around-one probe, are most valuable for those spectral regions.

This page intentionally left blank.

5.0 REFERENCES

Douglas, J.G., 1994, *Raman Program FY94 Test Plan*, WHC-SD-WM-TP-199, Rev. 0, Westinghouse Hanford Company, Richland, Washington.

Postma, A.K., J.E. Meacham, T.S. Barney, G.L, Borsheim, R.J. Cash, M.D. Crippen, J.M. Grigsby, D,W. Jeppson, M. Kummerer, J.M. McLaren, C.S. Simmons, B. C. Simpson, 1994, *Ferrocyanide Safety Program: Safety Criteria for Ferrocyanide Watch List Tanks*, WHC-EP-0691, Westinghouse Hanford Company, Richland, Washington.

Tseng, C., J. F. Ford, C. K. Mann, T. J. Vickers, *Wavelength Calibration of a Multichannel Spectrometer, Applied Spectroscopy*, Vol. 47, pp. 1808-1813.

Wodrich, D.D., 1994, *Tank Waste Remediation System Integrated Technology Plan*, DOE/RL-92-61, Rev 1, United States Department of Energy, Richland, Washington.

This page intentionally left blank.

9513358.1451

APPENDIX A
LLNL RAMAN SYSTEM SPECIFICATIONS

This page intentionally left blank.

APPENDIX A: LLNL RAMAN SYSTEM SPECIFICATIONS

The Raman system in the 305 building cold test facility was developed by Lawrence Livermore National Laboratory (LLNL) with support from DOE's EM-50 Office of Technology Development. The Raman system was specifically designed and packaged to be used for remote measurements in Hanford's hot-cells with tank waste materials, based on requirements sent to LLNL in FY-92 by WHC.

A block diagram of this Raman system showing the major components and layout within the "air tight" package is shown in Figure A-1. This diagram shows the a vertical profile of the backside of the cabinet. The relative positional dimensions and size of components within the enclosure are shown fairly accurately. The major components in the Raman system include:

- Cabinet
- Laser (monochromatic light source)
- Spectrograph with fiber-optic interface
- CCD detector array and driver electronics
- Computer system
- Air coolant and high-efficiency particulate air (HEPA) filter system
- Electrical power bus
- Fiber-optic bus panel
- Liquid-nitrogen auto-filler (not shown in Figure A-1)

The auto-filler was added to the LLNL Raman system to eliminate the daily requirement to manually replenish the CCD detector's liquid nitrogen coolant.

A.1 Cabinet

The Raman system cabinet provides a base for mounting all of the Raman components as well as functions as a contamination-free enclosure to keep dust and dirt contamination away from the Raman components. The system diagram in Figure A-1, which shows the vertical perspective of the cabinet, is fairly representative of the size and dimensions of the cabinet and Raman components. The diagram shows the internal cabinet view from the side of the cabinet that contains the large access door. The opposite side has the system interface panels (electrical and fiber-optic bus panels) and includes a window to view the computer monitor and shelf to hold the computer key board and spectrograph remote controller. The right side of the cabinet has a penetration for the vacuum valve connection and removable plexiglas panels for access to the computer disk drives and the detector controller controls. A penetration on the top is provided for the liquid-nitrogen fill tube. The disk and controller access holes are covered with plexiglass panels that are attached to the cabinet with Velcro and have a foam rubber seal around the perimeter of the opening in the cabinet to keep the penetration air tight. The controller and CPU were also mounted against the inner surface of the cabinet and are sealed with a similar foam

rubber gasket against the inner cabinet surface. Table A-1 gives detailed specifications for the Raman system cabinet.

The Raman system was designed to be operated with the cabinet doors closed. However, the following conditions require exposing the cabinet to its environment by opening the doors:

1. Replacing any individual component.
2. Turning the computer mainframe on or off by its power switch.
3. Turning the spectrograph on or off by its power switch.
4. Changing transfer fiber-optics.
5. Focusing or aligning the optical components (laser, spectrograph, detector).
6. Changing the laser band-pass filter.
7. Replacing the HEPA filter.
8. Access to all component electrical connections and fuses.
9. Evacuating the CCD detector dewar.

Removal of the Plexiglass cover which isolates the disk drives and the CCD detector controller switches will also allow introduction of particulates into the cabinet.

Adequate provisions were not made to conveniently interface a vacuum supply line to the CCD detector. The cabinet was modified to allow for this access by drilling a 3" diameter hole on the cabinet wall. This also exposed the cabinet to its environment when the vacuum system was on-line. The hole was taped shut when the vacuum port did not have to be accessed.

Table A-1. Specifications for Raman System Cabinet.

Supplier:	Rittal Corporation 3100 Upper Valley Pike Springfield, OH 45501 (800) 477-4000, fax (513) 390-5599
Enclosure Specifications	
Model number:	AK 1652
Dimensions (HWD):	120 cm x 120 cm x 40 cm
Weight:	108 Kg (empty)
Cabinet material:	1.5mm (16 gauge) sheet steel
Door material:	2.0mm (14 gauge) sheet steel
NEMA Rating:	NEMA 12
Cabinet Base (Plinth) Specifications	
Model number:	SO 2901
Dimensions (HWD):	10 cm x 80 cm x 37 cm
Castors model number:	SZ 2529 (1 set of 2 braking and 2 non-braking)

A.2 HEPA Filter and Cabinet Air Circulation

The purpose of the HEPA filter was to provide a source of clean room air to cool the Raman system components, particularly the argon-ion laser head which required forced-air cooling. As indicated in Figure A-1, the HEPA filter is mounted on the bottom of the cabinet over a large air duct. The laser head is mounted against the upper surface of the cabinet, directly on the upper cabinet air penetration. A 6 inch diameter, flexible air duct connects to this penetration on the outside of the cabinet. The flexible air duct is approximately eight feet long; a squirrel cage fan connected to the duct's other end draws cooling air through the cabinet.

When the cooling fan is on, it creates a slight vacuum within the cabinet. The vacuum draws air from below the cabinet bottom through the HEPA filter. This air then flows into the cabinet, around the laser power supply, and then through the laser head. There are no air dispersion baffles inside of the cabinet to deflect cool air to the other Raman components. A small computer cooling fan was installed to help circulate the incoming air so it could reach other components in the cabinet.

Figure A-1. LLNL System Diagram.

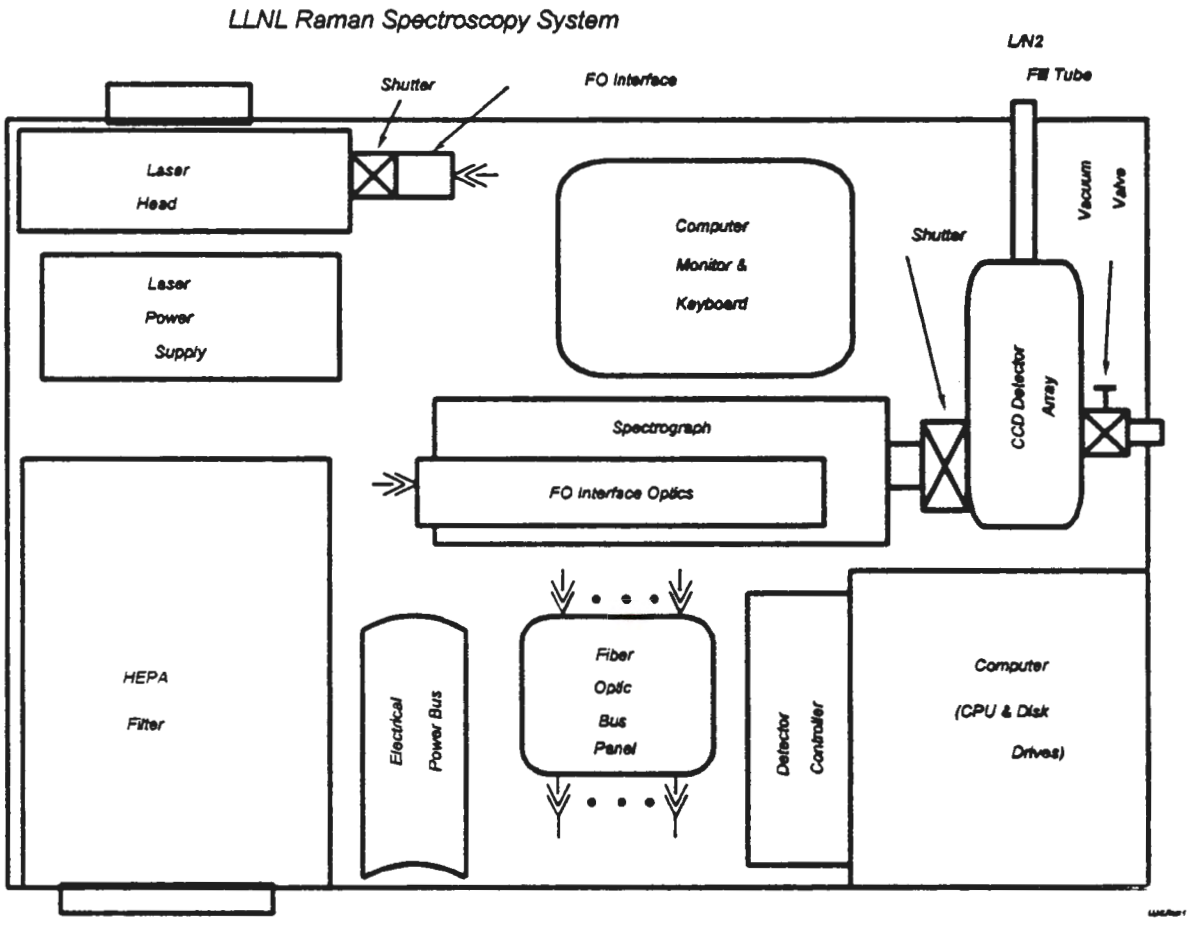

A.3 Computer System

The computer system was an AST Research, Inc., model 386SX/16 with a single hard drive and two floppy disk drives; Table A-2 outlines the computer's specifications. The computer's function was to operate the CCD detector array and store spectral data; the computer did not control the monochromator. The hard disk contained all of the system software programs, CCD detector control and data acquisition programs, and served as temporary storage of spectral data. Data were transferred to a floppy disk for off-line processing and archival. A plexiglass panel had to be removed to access the floppy disk drives.

The computer monitor was mounted behind a plexiglass panel that was sealed to the cabinet. The computer keyboard was external to the cabinet and connected to the CPU through a connector

mounted and sealed in the cabinet wall. A short, pigtail connector was used inside the cabinet between this connector and the CPU.

Table A-2. Specifications for Raman Computer System.

Supplier:

AST Research, Inc. 16215 Alton Parkway, Irvine CA 92713

Computer:

PN	500742-001
Model	AST Premium 386SX/16 Model 5v
Memory	8 Mbyte RAM (Extended)
Clock speed	16 MHz
Monitor	VGA
Hard Drive Capacity	80 Mbyte
Floppy drive A:	1.2 Mbyte, 5-1/4"
Floppy drive B	1.44 Mbyte, 3.1/2"
Operating system	MS-DOS version 5.0
Mouse	Logitech serial mouse

A.4 Laser System

The laser head was mounted immediately below the top panel of the Raman enclosure with the laser's cooling duct penetrating through the top panel. The laser head generated such a large quantity of excess heat that it could not be operated without forced-air cooling. Table A-3 lists the specifications for the laser.

The laser output was fitted with a remotely operated solenoid shutter and an adjustable focusing assembly equipped with an f/2, anti-reflection-coated focusing lens and an SMA-905 fiber-optic connector. The remotely operated solenoid shutter allowed the laser output to be completely blocked without having to turn off the laser. Use of the shutter avoided turning the laser off and the subsequent 30-minute warm-up time the laser required each time it was turned on. The adjustable focusing assembly consisted of an X (horizontal)-Y (vertical)-tilt translator containing focusing lens. The position of the focusing lens with respect to the end of the excitation-fiber ferrule was fixed; alignment consisted of adjusting the X, Y, and tilt orientation of the focusing lens to the laser beam to best couple the beam into the attached fiber-optic. A one-meter-long, 400-µm-diameter fiber-optic pig-tail was connected to the laser's SMA connector and carried the laser output to the system cabinet's front panel.

Table A-3. Specifications for Raman System Laser.

OMNICHROME, 13580 Fifth Street, Chino, California 91710
(714) 627-1594, (714) 591-8340 FAX

Model	543 argon ion
Beam diameter (@ 1/e2)	0.66 mm (TEM00)
	0.98 mm (TEM00)
Beam divergence	1. 1 mrad (TEM00)
	4.2 mrad (TEM00)
RMS noise (l0Hz to 10MHz)	<0.5%
Oscillation bandwidth	3 GHz
Mode spacing (c/2L)	349 MHz
Coherence length	10 cm
Linear polarization	Vertical +/- 5 degree
Minimum polarization ratio	250:1
Warm up time	30 minutes from startup
Recovery from STANDBY	< 1 msec
Beam pointing stability	<30 micoradians after warmup
Stability over 2 hours	<0.5 %
Cooling	Forced Air-Cooled
Power supply required	Model 160
Line voltage	230 Volts
Line frequency	60 HZ
Service current	20 Amp/Single Phase
Laser head weight	11.1 kg (25 lbs)

Laser Fiber-optic Interface Module:
Supplier:
OMNICHROME, 13580 Fifth Street, Chino, California 91710
(714) 627-1594, (714) 591-8340 FAX
Shutter:
Model: OES-001
Optical Interface:
Model: OFCVIS-001 tilt adjustor and SMA-905 fiber-optic connector
Model: OXY-001 X-Y translator

A.5 Spectrograph

The spectrograph was fitted with holographic gratings to disperse the wavelength content of the optical-fiber output onto the plane of the detector array which provides an electronic readout of the wavelength dispersed light. The spectrograph had three different gratings mounted on a turret that could be remotely rotated between three positions. This feature allowed the user to change the spectrograph's dispersion to generate a narrow, medium, or wide spectral window depending upon which of the three gratings was chosen. Table A-4 lists the specifications for the spectrograph.

The spectrograph input was through a fiber-optic interface module that was a custom LLNL design using commercially available quartz singlet lenses (designed for collimated light applications), micro-bench rails, and micro-bench component mounts. The two interface lenses were used in a collimating configuration (image and object planes at the lens focal planes) with a holographic laser line notch filter between the lenses. The notch filter selectively attenuated the laser light while allowing the Raman shifted light to pass into the spectrograph.

The spectrograph was a Czerny-Turner based optical system with an input slit, a collimating mirror, diffraction grating, and focusing mirror. The output of the spectrograph was focussed on the surface of the CCD detector array chip. The spectrograph was controlled through a remote controller. The input slit width, grating selection, and grating position were controllable variables. A digital readout on the control box provided alpha-numeric information for the operator. The controller was connected to the spectrometer through a sealed bulkhead connector in the front cabinet wall.

Table A-4. Specifications for Raman System Spectrograph.

Supplier:

Chromex Inc., 2705-B Pan American NE, Albuquerque, NM 87107
(505) 344-6270, (505) 344-6095 FAX

Specifications:

(Assume a 1200 g/mm grating in first order and a 20 micron slit width 5mm slit height)

Model	250IS with Retro-Illumination Option
Optical Configuration	Czerny-Turner

(with proprietary toroidal collimating and focusing mirrors providing aberration-corrected flat field stigmatic imaging performance)

Useful focal field area	10 mm x 20 mm Fully resolved 12 channels using 100μm diameter fibers on 500μm centers with interchannel crosstalk of $<10^{-3}$
Focal length	250 mm, 330 mm from mirror to detector
Aperture ratio	f/4.0
Reciprocal linear dispersion	2.5 nm/mm
Slits	straight bilaterally adjustable, 10-2000 micron, nominal 16 mm height
Wavelength accuracy	± 0.15 nm
Wavelength precision	± 0.05 nm scanning from same direction
Wavelength range	180 nm to 10μm (standard)
Resolution	0.15 nm Full width at half maximum
Apparent Magnification	1.3 (330/250)
Construction	Single-piece cast aluminum base
Footprint	22.5 cm x 42 cm
Weight	13.5 kg

A.6 CCD Array Detector

The CCD detector provided the spectral readout of the wavelength-dispersed light from the spectrograph. As shown in Figure A-1, this detector contained a vacuum insulated, liquid-nitrogen dewar and a shutter. The detector was mounted at the output focal plane of the spectrograph (the spectrograph has not exit slit). See Table A-5 for the CCD detector specifications. The detector array's horizontal axis was aligned parallel with the dispersion axis of the spectrograph. This allowed the vertical pixels of the array to be binned, that is, added together to produce a single value. The best signal-to-noise ratio for Raman measurements can be obtained by judiciously binning only that vertical region of the array covered by the spectral image.

The CCD detector chip was mounted on a cold finger inside the dewar that contains liquid nitrogen. This mount cold finger is in contact with the liquid nitrogen and a thermoelectric cooler/heater that allowed the temperature of the chip to be set and maintained at any temperature between -80°C and -130°C.

The CCD detector is operated through software from the computer system. The detector controller provides signal conditioning and interfacing between the detector and the computer with the exception of the temperature control which was solely a function of the CCD detector controller. A removable plexiglass panel allowed the operator access to the control panel on the detector controller, on/off, and temperature control functions. The controller also contains a temperature status light that indicates when the temperature setpoint is reached by the detector

chip. The controller can operate a number of different detector systems. The controller "personality" for a particular detector is set with mechanical switches internal to the controller. Once set, these switches are not changed, unless the detector model is changed.

Liquid nitrogen is added to the detector's dewar through the fill tube which extended through the top of the cabinet. The vacuum valve connects the dewar to a vacuum system for periodic evacuation. The dewar uses a vacuum to isolate the CCD and cold finger from ambient air. If the vacuum is lost, the system would not hold temperature, which could cause fogging of the windows in the detector package. A vacuum level of around 10×10^{-3} Torr was needed to prevent condensation and contaminants from collecting on and destroying the CCD. Access to the vacuum valve required opening the large cabinet door.

Table A-5. Specifications for Raman System CCD Detector.

Detector:

Princeton Instruments, Inc, 3660 Quakerbridge Road, Trenton, NJ 08619
(609)587-9797, (609)587-1970 FAX

Model	LN-CCD/1024 TKB back illumination, standard format
Format	1024x1024 pixels (24 x 24 μm/pixel)
Full Well Capacity	≥ 5000,000 electrons
Readout Noise	4-6 electrons
Spectral Range	400-1080nm
Dynamic Range	16-bits (16355 maximum signal)
Response Non-linearity	≤ 1%
Response Non-Uniformity	Less than ± 6% over entire CCD area, except for blemish regions. Less than ± 3% with binning.
Operating temperature	-120°C (adjustable -80 to -130°C)
Typical Dark Charge	< 0.00025 electrons/pixel-second
Scan rate	100 kHz
Readout time	175 ms
Controller	ST-130
CSMA software version	2.3a

A.7 Fiber-Optic Bus Panel

The fiber-optic bus panel allowed the interchangeable use of several probe types including six-around-one and two fiber probes. The panel consisted of SMA 905 panel feed-throughs that coupled the laser and spectrograph fiber-optic cable on the inside of the cabinet with probe fiber-optic cables on the outside of the cabinet. The spectrograph fiber cable consisted of six 400μm diameter fibers individually terminated at one end with SMA connectors; the fibers at the spectrometer end were stripped to the cladding, closely packed in a single line, and epoxied into a one-inch-diameter aluminum mandrel. The line of fibers was aligned perpendicular to the

spectrograph dispersion axis (parallel to the spectrograph input slit) to allow vertical pixel binning for the two dimensional detector. Table A-6 shows the specifications for the fiber-optics used in the Raman system.

Table A-6. Specifications for Raman System Fiber-Optic Interface.

Ensign-Bickford Optics Co., 150 Fisher Drive, Avon, CT 06001
(203)678-0371, (203)674-8818 FAX

Product Type	400μm CC905 radiation hardened
Core Diameter	400μm
Clad Thickness	~15μm
Attenuation	(not given)
Reel No.	A2536ACS
EBOC Order#	4058

A.8 Liquid-Nitrogen Auto-filler

Figure A-1 does not show the liquid-nitrogen autofiller system that was added to the Raman system by WHC. The autofiller keeps the CCD's liquid-nitrogen dewar full by periodically adding liquid nitrogen. This eliminated the need for manual filling which was required approximately every 12 hours or sooner when the CCD detector system was being used. When the Raman system was not in use, the CCD detector temperature controller was switched off to conserve liquid nitrogen.

The autofiller consisted of three modules: liquid-nitrogen source dewar, autofiller head, controller module, and insulated hose/valving. The input end of the auto-filler hose was attached to the liquid-nitrogen dewar with an air-tight fitting. This fitting also contained two over-pressure release valves. Dewar pressure was supplied by the inherent slow boil-off of liquid nitrogen.

An insulated, flexible tube connected the source dewar to the auto-filler head. The auto-filler head was a small box with a stainless-steel tube that was inserted into the CCD's liquid-nitrogen dewar.

The controller provided the auto-filling timing action, valve control interface, and temperature sensing needed in the auto-filling operation/cycle. An auto-fill cycle was triggered by a timer in the auto-filler controller. The controller opened a valve in the auto-filler head and the pressure in the storage dewar forced liquid nitrogen into the CCD dewar through the flexible hose and down through the rigid pipe on the auto-filler head. The auto-filler head had a thermal sensor which terminated the filling action when a setpoint temperature level in the auto-filler head was passed. The timer then counted down until the time-out time interval was reached and repeated the filling cycle.

Table A-7. Specifications for Raman System Liquid-Nitrogen Auto-Filler System.

Supplier: JC Controls, 1069 Westridge Ave., Danville, CA 94526
(510) 837-6677, (510) 743-0529 FAX

Specifications:

Model:	SNTDF-6 Liquid Level Controller
Cabinet:	5.4cm H x 15.6 m W x 17.1cm D
Power:	105-125 VAC, 50-60 Hz
Fuse:	3 amp
Sensor:	Encapsulated 4mm OD x 9.5mm long, on 24cm glass sheathed lead wires. Unlimited length possible by splicing 2 conductor #22 wire. Sensor will negotiate 90° curves in 6.4mm OD x 0.9mm wall tubing with a radius as small as 38 mm.

This page intentionally left blank.

9513358.1458

APPENDIX B
RAMAN SPECTRAL DATA PROCESSING

This page intentionally left blank.

APPENDIX B: RAMAN SPECTRAL DATA PROCESSING

The generic steps used to collect and process Raman spectra were: (1) collect dark-charge, white-light, probe, neon wavelength reference, and sample spectra using FSU's *RCAL* data-collection software, (2) treat each raw spectrum to remove the dark-charge and CCD detector characteristics ("dark/white correction"), (3) subtract the probe spectrum (consisting of the probe's Raman silica response) from the dark/white corrected spectrum, (4) remove any luminescence background, and (5) convert the x-axis to delta wavenumbers (cm^{-1}) using the neon spectrum and the laser's excitation frequency. Additional steps might include, where applicable (a) averaging multiple, sequential dark/white corrected spectra that were obtained for a single material within a given spectral window and (b) remove extraneous noise using a maximum likelihood smoothing algorithm.

The *RCAL* data-collection software automatically performs the dark/white correction upon collection of the raw spectrum (the *RCAL* software saves both the raw and corrected spectral data files). Spectral data files were exported from the *RCAL* file format as text files and subsequently imported into Galactic Industries Corporation *GRAMS/386* spectral data processing software for the subsequent processing steps.

B.1 Rationale for Raman Spectral Data Processing Steps

This section outlines the logic behind the Raman spectral data processing steps. A "raw" Raman spectrum may be represented as

$$\begin{matrix} raw \\ spectrum \end{matrix} = \left(\begin{matrix} \text{"true"} \\ spectrum \end{matrix} + \begin{matrix} silica \\ response \end{matrix} + L \right) \times \left(\begin{matrix} spectrometer \\ response \\ function \end{matrix} \right) + \begin{matrix} dark \\ signal \end{matrix}$$

where *raw spectrum* is the untreated spectrum as it is obtained from the spectrometer detector, *"true" spectrum* is that portion of the spectral signal attributed only to the Raman scattering coming from the sample, *silica response* is the Raman response from the silica fiber-optics, L is other spectral processes (e.g. luminescence), *spectrometer response function* expresses how the spectrometer changes the Raman signal as it passes through the fiber-optic receiving fiber, spectrometer, and CCD detector, and *dark signal* is the signal present when no light strikes the detector.

Recovering the "true" spectrum provides the rationale for the various spectra collected in addition to the original raw spectrum. A tungsten lamp (*white-light*) spectrum approximates the

spectrometer response function, and the dark-signal spectrum (composed chiefly of the CCD DC offset, collected with the CCD shuttered close) provides the dark signal function.

In addition to compensating for the spectrometer response function and the dark signal, the silica fiber itself adds a silica Raman signal to the sample spectrum. This is an additive feature, so we must subtract the silica fiber Raman spectrum from the "true" spectrum to recover the Raman signal due to the sample alone. The operator collects the silica Raman spectrum with the fiber-optic probe in a Raman inactive material such as sodium chloride; the resulting Raman spectrum is due to the silica fiber alone. Since the silica spectrum is subtracted from the dark/white-corrected sample spectrum, noise in the silica spectrum will contribute to the noise in the silica-subtracted spectrum. To reduce the noise contributed by the silica spectrum, the silica spectrum should be time-averaged over a longer time than the sample spectrum.

Luminescence in a Raman spectrum is usually manifest as a broad, arched, or sloping background. Luminescence generally consists of broad-band spectral components that are readily discernable from the narrow-band Raman signals. Luminescence background is usually removed by subtracting a polynomial fit through the background. Alternatively a series of short, linear segments may be fitted through the background. There are two difficulties with this procedure: (1) if the selected background fit does not model the luminescence exactly, then the subtraction will leave artifacts in the resulting spectra and (2) the noise component from the luminescence remains. To avoid these two difficulties, the excitation wavelength should be chosen to minimize the generation of luminescence in the samples.

The chief aim of performing these spectral subtraction and ratioing operations is to recover accurately the Raman signals contained in the raw Raman spectrum. This aim must be achieved without introducing artifacts into the resulting spectrum. At least two points must be observed when performing the subtraction steps: (1) negative peaks are not permitted (2) spectral features (other than noise) with a bandwidth narrower than the instrument band-pass are not permitted. The appearance of either in a spectrum indicates an artifact generated during a spectral data subtraction step.

Spectral smoothing operations may also add artifacts to the resulting spectrum. The desired end-result of a spectral smoothing operation is to reduce the high-frequency noise in the spectrum while leaving intact the frequency components that legitimately contribute to the spectrum. A common form of noise encountered with CCD detectors are so-called "cosmic events". These are caused when a high-energy photon (e.g. gamma ray) or high-energy particle (e.g. alpha or beta radiation) strikes the detector. This form of *impulse noise* will generate artifacts upon smoothing because the resulting spike, while mostly composed of high-frequency components, will also contain low-frequency components in the spike's "wings". Upon smoothing, these low-frequency components will remain behind and possibly cause a false peak in the smoothed spectrum. "Cosmic events" must be removed, or better yet prevented from occurring, prior to smoothing operations. For the work reported in this study, cosmic events were not a problem.

9513358.1460

APPENDIX C
FIBER-OPTIC FILTERS

This page intentionally left blank.

APPENDIX C: FIBER-OPTIC FILTERS

C.1 Filter Specifications

The fiber-optic cable connectors use butt coupling between the polished ends of the connector ferrules. With an SMA-905 connector, the fiber ends are glued in the center of either a ceramic or metal ferrule. The SMA-905 connectors allow the insertion of small diameter, thin optical filters between the finished ends of SMA-905 connectors. The filter specifications for a doubled Nd:YAG laser (532nm line) are shown below in Tables C-1 and C-2. The band-pass filter, centered over the laser line, attenuates the optical fiber silica Raman signal. The long-wave pass filter blocks laser light (reflected from probe and sample surfaces) from entering the detector fiber where it can again generate silica Raman scattered light.

The filter coatings that produce the optical characteristics are soft and were protected with bonded glass covers. The filter were constructed by depositing coatings on a large glass substrate and cutting small 3mm diameter circles from this bulk material. Each filter has a thin cover glass bonded to the substrate to form the filter sandwich.

Table C-1. 532 Long-Wave Pass Optical Filter.

Long-Wave Pass Optical Filter For 532nm Doubled Nd:YAG Laser Line	
Transmittance at 532 nm	less than 10%
Transmittance of 545 to over 650 nm	greater than an average of 80%
Filter diameter	3 mm
Filter thickness	0.5 mm ± 0.1 mm
Substrate material	BK-7 glass or equivalent

Assumes incident light is normal to the filter surface.

Table C-2. 532 Laser Band-Pass Optical Filter.

Band-Pass Optical Filter For 532nm Doubled Nd:YAG Laser Line	
Center Wavelength	532nm ± 1.5mm
Full Width At Half Maximum (FWHM)	6nm ± 1.5nm
Peak Transmission	greater than 75%
Long Wave Blocking	20 dB from 545 nm to over 685 nm
Filter diameter	3 mm
Filter thickness	0.5 mm ± 0.1 mm
Substrate materials	BK-7 glass or equivalent

Assumes incident light is normal to the filter surface.

C.2 Filter Characterization

To attenuate the Raman scattering generated in the fiber-optic Raman probes, the incorporation of optical filters near the distal ends of the WSRC chisel-tip probe and the NIR diffuse-reflectance probe was evaluated. Two filters with different optical functions were used – a laser band-pass filter in the excitation leg and a long-pass filter in the collection leg of the probes.

The laser band-pass filter should remove the silica-Raman signals generated in the excitation leg of a fiber-optic probe and prevent the silica Raman from the excitation leg from "contaminating" the sample spectrum due to "cross-talk" with the collection fiber. Ideally, the laser band-pass filter will pass only the excitation wavelength with maximum efficiency and with a band-pass narrow enough to exclude the excitation-fiber silica-Raman background.

In the collection fiber, reflected laser light and Rayleigh-scattered light may also induce silica-Raman signals that can add a silica-Raman background to the sample spectrum. The long-pass filter should ideally reject all the laser and Rayleigh-scattered light and pass a maximum amount of the wavelengths longer than the excitation wavelength. Neither filter should contribute any additional luminescence to "contaminate" the sample spectrum. To determine how suitable these filters are for fiber-optic Raman measurements, the transmission and luminescence characteristics of the filters employed in the fiber-optic probes were measured.

C.2.1 Filter Transmission Characteristics

Figures C-1 and C-2 and Table C-3 show the transmission characteristics for the 514.5- and 532.2-nm filter sets. The following procedure was used to produce these spectra: (1) a raw transmission spectrum was obtained by transmitting a white-light source through a WSRC chisel-tip probe equipped with a filter body containing the test filter; the filtered output was imaged on the entrance slit of the Raman spectrometer (holographic notch-filter removed) and the resulting spectrum recorded; (2) a white-light spectrum was collected under identical conditions with the filter removed from the filter body; (3) the filter's raw transmission spectrum was then ratioed with the white-light spectrum to produce the corrected transmission spectrum; (4) a neon spectrum was recorded for wavelength calibration. Additional determinations of the laser band-pass filter transmission efficiencies were made by using a laser-power meter to measure the laser power transmitted through the probe with and without the filters in place. Index-matching grease was not used on the filter/fiber junctions for these measurements. Table C-4 details the experimental conditions used for the filter characterizations.

One major observation from Figures C-1 and C-2 is that the transmission efficiency of the 532.2-nm long-pass filter does not appear to be as good as that for the 514.5-nm filter. Also, Table C-3 indicates a discrepancy between the percent transmission for the 514.5-nm laser bandpass filter as measured from the transmission curve (50%) and direct measurement using an argon-ion laser and laser-power meter (83%). The reason for this discrepancy is not known. The curves shown in Figures C-1 and C-2 were measured with the filters in the fiber-optic probe; the actual filter transmission characteristics for the "bare" filters may be somewhat different from those curves in the figures. The use of index-matching gel should enhance the transmission characteristics of these in-line filters by minimizing Fresnel reflections at the fiber-optic/filter interface.

Table C-3. Transmission Characteristics for Fiber-Optic Raman Probe Filters.

Characteristic	514.5 nm	532.2 nm
Laser Band-Pass Filters		
Maximum transmission wavelength	513.3 nm	532.6 nm
Full-width-at-half-height	6.3 nm	8.7 nm
Transmission efficiency at maximum transmission wavelength[a]	69%	58%
% transmission at laser wavelength[a]	50%	57%
% transmitted laser light[b]	83%	58%
Long-Pass Filters		
10% transmission wavelength	512.3 nm	529.4 nm
% transmission at laser wavelength	13%	12%
Maximum % transmission (wavelength)	75% (596.5 nm)	68% (612 nm)

[a]From Figures C-1 and C-2.

[b]Ratio of transmitted laser power with and without filter in place as measured with laser power meter.

Table C-4. Experimental Conditions for Determining Raman Probe Filter Transmission Characteristics.

Parameter	Setting
Probe	Westinghouse Savannah River Company two-fiber "chisel-tip" probe equipped with filter bodies
White-light source	tungsten-halogen lamp
Spectrometer slit width	25 µm
Spectrometer slit height	15 mm
Grating	300 g/mm
Resolution	1.7 nm
Spectral window center wavelengths	514.5-nm filters: 600 nm 532.2-nm filters: 570 nm

Figure C-1. Laser Bandpass and Long-Pass Filter Characteristics for 514.5-nm Excitation. (Vertical dashed line indicates laser wavelength.)

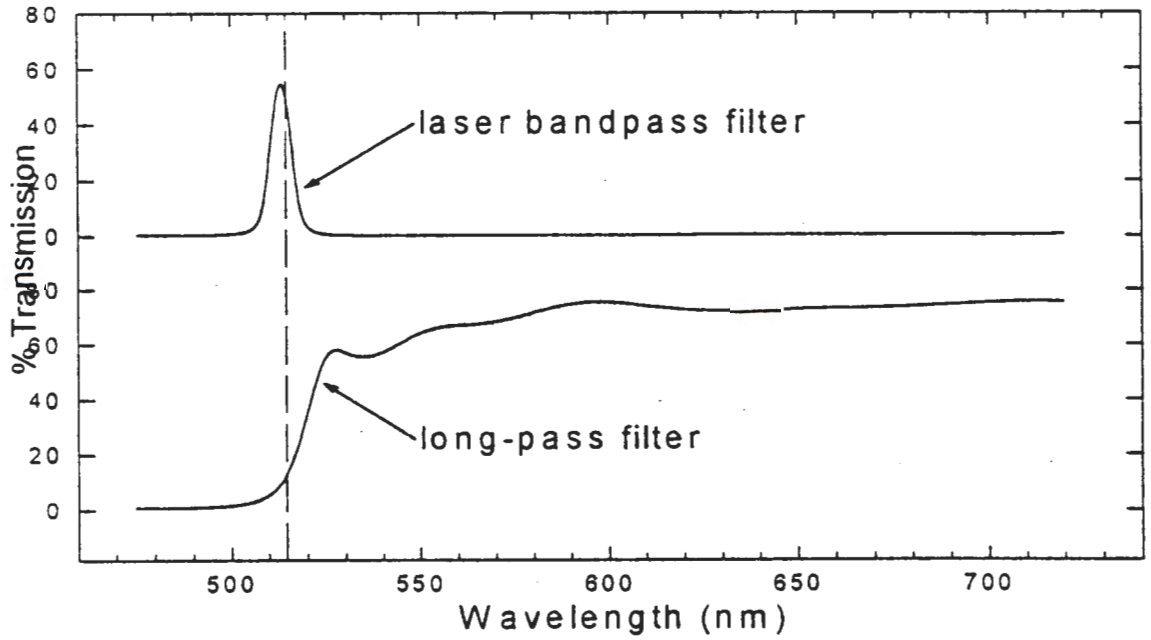

Figure C-2. Laser Bandpass and Long-Pass Filter Characteristics for 532.2-nm Excitation. (Vertical dashed line indicates laser wavelength.)

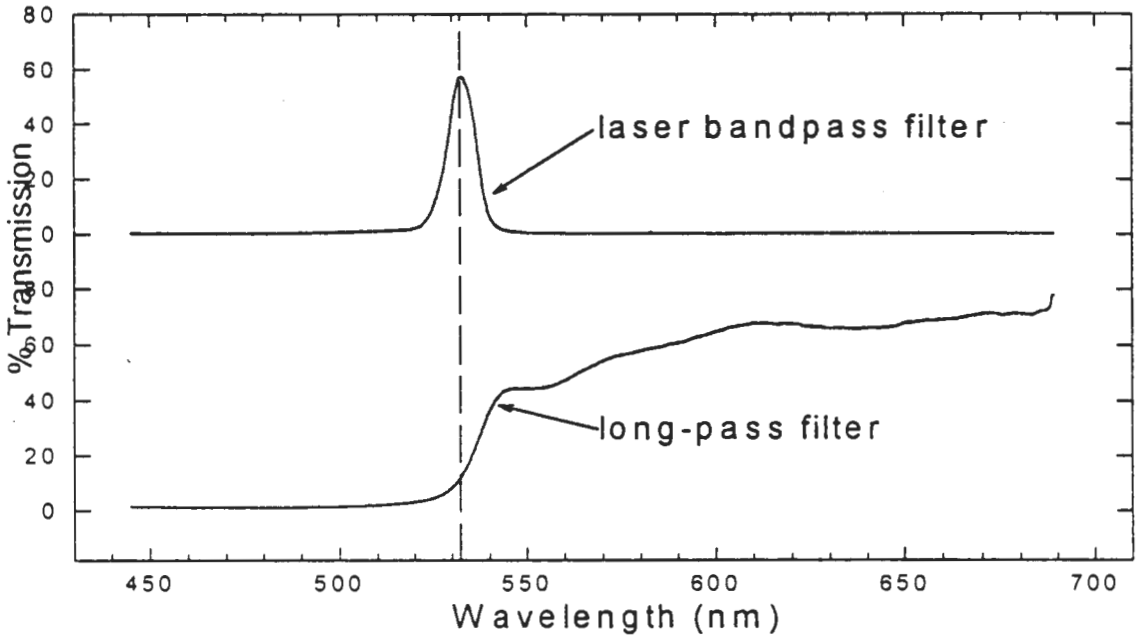

C.2.2 Filter Luminescence Characteristics

Concerns were raised that the in-line filters may generate enough luminescence under laser excitation to add a spectral background to the Raman spectrum; therefore, attempts were made to collect luminescence spectra for the 514.5-nm and 532-nm in-line filter sets. Figure C-3 shows what appears to be luminescence spectra for the in-line optical filters. To collect these spectra, standard Raman spectra were acquired with the filter of interest as the target. The output of the appropriate laser (514.5-nm argon-ion for the 514.5-nm filters and the doubled Nd-YAG for the 532.2-nm filters) was coupled to the central fiber of a six-around-one fiber-optic probe. Each filter was illuminated with the probe set at 45° to the normal to the sample surface to minimize specular reflectance from the sample surface; the probe tip was approximately 7mm from the viewing point on the sample surface. The surrounding six fibers of the probe collected the scattered light and any luminescence from the sample surface and returned the light to the monochromator. The monochromator's 1200-g/mm grating was used as the dispersive element.

The filter luminescence spectrum was obtained by subtracting a silica-Raman reference spectrum from each recorded filter spectrum to remove the Raman signal of the optical fiber from the spectrum.

Because of the variability in the sample geometry, quantitative statements cannot be made regarding the magnitude of the luminescence from these filters. However, since the filters' optical pathlengths are short (ca. 500 μm) and any luminescence will be isotropically emitted, it is not anticipated that filter luminescence will be a major background or noise source in Raman spectra acquired using probes containing these filters. Indeed, experience with such filtered probes has not revealed any background luminescence that can be attributed to the filters.

Figure C-3. Probe Optical-Filter Luminescence upon Laser Excitation. (A) 514.5-nm Laser Bandpass Filter, (B) 514.5-nm Long-Pass Filter, (C) 532.2-nm Laser Bandpass Filter, (D) 532.2-nm Long-Pass Filter.

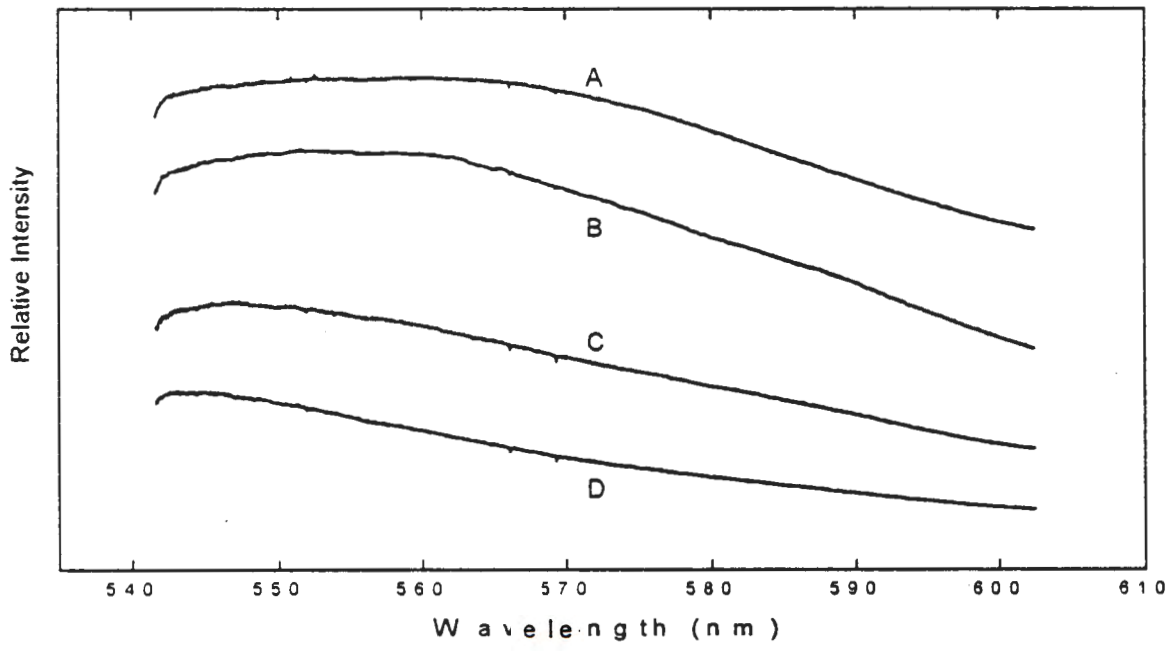

This page intentionally left blank.

9513358.1465

APPENDIX D
OPTICAL ALIGNMENT PROCEDURES

This page intentionally left blank.

APPENDIX D: OPTICAL ALIGNMENT PROCEDURES

This section outlines the procedures used to optically align the Lawrence Livermore Raman system. The system's hardware and software are outlined in Section 2.0 of this document.

D.1 Alignment of Laser/Fiber-Optic Interface

The laser/fiber-optic interface consisted of a commercially available (Omnichrome, Inc.) X (horizontal)-Y (vertical)-tilt translator containing a 5-mm diameter, 10-mm focal length, anti-reflection-coated focussing lens. The position of the focussing lens with respect to the end of the excitation-fiber ferrule was fixed, so alignment consisted of adjusting the X, Y, and tilt orientation of the focussing lens to the laser beam to best couple the beam into the fiber-optic. This was done by coupling the distal end of the excitation-fiber pigtail to a laser power meter. With the laser on and the laser shutter open, the X, Y, and tilt screws were adjusted to achieve a maximum power reading on the laser power meter, then tightened the translator's locking screws to lock the translator in position.

D.2 CCD Detector Rotational Alignment and Focussing

This step aligns the vertical axis of the CCD detector to the spectrometer's entrance slit. To perform this alignment, the optical components were removed from monochromator's entrance slit and room light (mercury arc lamp) was allowed to illuminate the entrance slit. The following instrument parameters were used: 20-μm entrance slit width, 1200-groove/mm grating, and 546-nm spectral position. The Princeton Instruments, Inc., *CSMA* software was used to obtain three binned strips, each strip 50-pixels wide, near the top, center, and bottom of the CCD. The camera housing was then rotated until the top and bottom strips aligned vertically (often the center strip did not align with the top and bottom strips because of the monochromator's coma), then locked the detector's rotational axis in place with the appropriate set screw.

The purpose of the detector focussing step is to position the detector at the spectrometer's focal plane and thus to achieve the maximum spectral resolution. This step was performed after completion of the CCD detector rotational alignment and the CCD detector was focussed using the same experimental conditions for the rotational alignment. The detector mount incorporates a micrometer adjustment to move the detector parallel to the spectrometer's optical axis. The micrometer was adjusted to move the detector until a maximum separation was achieved between the mercury lines observed in the spectrum. It was easier to visually determine the best separation between adjacent mercury lines rather than attempting to visually determine when the narrowest line width was achieved. Maximum resolution was obtained with the detector positioned as close to the spectrometer housing as possible; since the detector could not be situated any closer to the spectrometer, it was not ascertained whether or not the detector was indeed at the spectrometer's image plane. After obtaining the best available spectral resolution, the CCD detector's translational set screw was tightened.

D.3 Transfer Optics Alignment and Focussing

The Raman spectrometer transfer optics consisted of an aluminum mandrel holding the ends of the probe collection fibers, a collimating lens, a holographic notch filter, a focussing lens, and a front-surface turning mirror to direct the collected light into the monochromator. All these components were mounted in individual component carriers that were attached to a miniature three-rail optical bench. A light-tight box attached to the side of the monochromator housed the entire transfer optics assembly.

Alignment and focussing of the fiber-optic/spectrometer transfer optics ensures that the light emitted from the spectrometer end of the fiber-optic probe is coupled into the spectrometer with maximum efficiency. This step was performed after the detector alignment steps of Section F.2. The initial step consisted of removing the holographic notch filter from its component carrier; any other optic components displaced during detector alignment steps were repositioned on the mounting rails of the transfer optics housing.

The aluminum mandrel holding the spectrometer end of the collection fibers was visually positioned to align the fiber ends as nearly vertical as possible. With the excitation laser on, and the probe aimed at a reflective target (e.g. a KCl pellet), the collimating lens was positioned so that the fiber ends were approximately at the focal point of the collimating lens. Collimation was visually checked with a white card by placing the card after the collimating lens and moving the card along the optical axis. The lens position was adjusted until the collimated image size on the card appeared constant with distance from the lens.

The focussing lens and turning mirror were then visually adjusted to focus an image onto the entrance slit of the monochromator. At this point, the laser was shuttered and a neon lamp was aimed at the distal end of the fiber-optic probe. Using the *CSMA* software, neon spectra were acquired in the "free-run" mode with the following instrumental parameters: 20-μm slit width, 1200-groove/mm grating, and monochromator wavelength at about 600 nm. Working "backwards" through the transfer optics, the turning mirror, focussing lens, and collimating lens were adjusted to achieve best resolution and maximum peak height. When this initial optimization was completed, a final rotational adjustment of the fiber mandrel was made to maximize line intensity. Final adjustments of the optical components (including adjustment in the plane perpendicular to the optic axis) were performed with 200-μm slits while monitoring several neon line shapes; the desired line shape was symmetric with a flat top. (Due to monochromator coma, this line shape can only be obtained over a fairly narrow spectral region.) Typically, the instrument resolution check was repeated with both 20-μm and 200-μm slits again to ensure that the optimal alignment of the transfer optics was achieved.

The final step in aligning the transfer optics was to reinsert the holographic notch filter and rotationally tune the filter for minimum Rayleigh intensity. This step was performed by monitoring the Rayleigh line with the laser on and the fiber-optic probe aimed at a KCl target; the filter was

rotated in its component holder to minimize the height of the Rayleigh line while maximizing the probe-silica Raman bands on the Stokes side of the Rayleigh line.

This page intentionally left blank.

9513358.1468

APPENDIX E
TANK SIMULANT CHEMICAL DATA

This page intentionally left blank.

APPENDIX E: TANK SIMULANT CHEMICAL DATA

Cold testing is one of the steps in the development of instrumentation for use with HLW materials. This normally involves the use of both pure material samples and simulant samples. Although there are significant differences between simulant and real materials, testing with simulants provides data that can be used to assess basic technology and system performance issues.

In the cold test work with the Raman spectroscopy system, four tank waste simulants were used. These simulants represent a portion of the range of optical, physical, and chemical properties suspected to be present in real tank wastes. How accurately these materials actually simulate the Raman response from real tank waste is yet to be fully determined.

(1) BY-104 simulant (Table E-1): The BY-104 simulant represents the salt-cake material found on the surface of the waste in tank BY-104. The simulant ranges in color from light tan to brown with increasing water content. The material ranges from a coarse, loosely aggregated sand when dry to a gritty paste when wet.

(2) T-Plant simulant, top fraction (Table E-2): The T-Plant ferrocyanide flow sheet was used to generate the simulant; this material is the top ca. 90 weight percent of the centrifuged product. Actual tank waste produced from the T-Plant flow sheet were originally deposited in the TY tank farm. The simulant is a sludge with a tan color and the consistency of peanut butter.

(3) T-Plant simulant, bottom fraction (Table E-3): This material is the bottom ca. 10 weight percent of the centrifuged product generated in conjunction with the T-Plant top fraction. This simulant is a sludge with a dark tan color and the consistency of peanut butter.

(4) SY-101 simulant (Table E-4): This material simulates the SY-101 tank waste. Tank SY-101 is classified as a complexant concentrate tank. This simulant contains a representative amount of organic carbon in the form of tetrasodium EDTA.

In general, all of these simulants are dark colored, suggesting strong optical absorption for the visible wavelength region. Each simulant also exhibited some unique optical (absorption, color, scattering, etc.) features so that the leakage of light through samples of equal thickness was different for each material. This had an impact on how the fiber-optic probes are used with these samples; some samples will be more sensitive to ambient light for in situ applications.

Table E-1. BY-104 Salt-Cake Simulant.

COMPOUND	MOLECULAR WEIGHT	WEIGHT %
$NaNO_3$	85.0	81.8
$NaAlO_2$	82.0	7.5
NaOH	40.0	1.7
Na_2SiO_3	122.1	1.5
$Fe(NO_3)_3$	241.9	1.0
Na_3PO_4	163.9	0.7
$Ca(NO_3)_2$	164.1	0.4
$Mg(NO_3)_2$	148.3	0.2
$Mn(NO_3)_2$	179.0	0.2
H_2O	18.0	approx. 5

Table E-2. Composition of T Plant Top Simulant.

COMPOUND	MOLECULAR WEIGHT	WEIGHT %
$(NH_4)_2SiF_6$	178.2	9.4
$NaNO_3$	85.0	7.2
Na_3PO_4	163.9	6.6
$Fe(OH)_3(Fe_2O_3)$	106.9	4.9
$Na_2NiFe(CN)_6$	303.9	2.6
$NaNO_2$	69.0	2.2
$Cr(NO_3)_3$	238.0	1.5
Na_2SO_4	142.0	0.6
$BiPO_4$	304.0	0.5
$Zr_3(PO_4)_4$	653.5	0.1
$CsNO_3$	194.9	Trace
H_2O (bound)	18.0	1.2
H_2O (free)	18.0	69.0

Table E-3. Composition of T Plant Bottom Simulant.

COMPOUND	MOLECULAR WEIGHT	WEIGHT %
$BiPO_4$	304.0	31.2
$(NH_4)_2SiF_6$	178.2	5.2
$NaNO_3$	85.0	2.5
$Fe(OH)_3$	106.9	2.1
$Na_2NiFe(CN)_6$	303.9	0.8
$NaNO_2$	69.0	0.8
$Cr(NO_3)_3$	238.0	0.7
Na_2SO_4	142.0	0.3
$Zr_3(PO_4)_4$	653.6	0.3
$CsNO_3$	194.9	Trace
H_2O (bound)	18.0	0.6
H_2O (free)	18.0	45.0

Table E-4. Composition of SY-101 Simulant.

COMPOUND	MOLECULAR WEIGHT	WEIGHT %
$NaNO_2$	69.0	16.2
$NaAlO_2$ $(2H_2O)$	118.0	14.5
$NaNO_3$	85.0	13.4
NaOH	40.0	7.1
Na_2CO_3	106.0	6.7
Na_4EDTA $2H_2O$	??	5.5
$Cr(NO_3)_3$ $9H_2O$	400.0	3.2
Na_3PO_4 $12H_2O$	379.9	2.6
NaCl	58.5	1.3
KNO_3	101.1	0.9
Na_2SO_4	142.0	0.6
$Fe(NO_3)_3$ $9H_2O$	403.9	0.2
$Ca(NO_3)_2$ $4H_2O$	236.1	0.1
$Ni(NO_3)_2$ $6H_2O$	290.7	0.1
NaF	42.0	0.1
$ZnCl_2$	136.4	Trace
$CsNO_3$	194.9	Trace
$Sr(NO_3)_2$	211.6	Trace
H_2O (free)	18.0	27.51

This page intentionally left blank.

DISTRIBUTION (cont.)

Number of Copies		
ONSITE	Westinghouse Hanford Company (cont.)	
	W. F. Zuroff	R1-30
	Central Files (2)	L8-04
	~~Document Processing and Distribution~~	~~L8-15~~
	EDMC	H6-08
	OSTI (2)	L8-07
	Tank Farm Information Center	R1-20

THIS PAGE INTENTIONALLY
LEFT BLANK

DISTRIBUTION

Number of Copies

OFFSITE

4	U. S. Department of Energy, Headquarters 12800 Middlebrook Road Germantown, Maryland 20874 R. Geiser K. Lang C. Purdy S. Wolfe
1	U. S. Department of Energy, Morgantown Energy Technology Center P. O. Box 880, 3610 Collins Ferry Road Morgantown, West Virginia 26507-0880 C. Nakaishi
1	U. S. Department of Energy, Savannah River Operations Office P. O. Box A Aiken, South Carolina 29808 T. Temple
1	U. S. Department of Energy, Science Applications International Corporation 12850 Middlebrook Road Trevion I, Suite 300 Germantown, Maryland 20874 R. Daniels

THIS PAGE INTENTIONALLY
LEFT BLANK

DISTRIBUTION (cont.)

Number of Copies

OFFSITE

2 U. S. Department of Energy,
Science Applications International Corporation
2030 Century Blvd. Suite 200B
Germantown, Maryland 20874

H. Sutter
P. Szerzen

6 Tank Advisory Panel Members

C. S. Abrams
1987 Virginia
Idaho Falls, Idaho 83404

D. O. Campbell
102 Windham Road
Oak Ridge, Tennessee 37830

F. N. Carlson
6965 North 5th West
Idaho Falls, Idaho 83401

D. T. Oakley
409 12th Street SW, Suite 310
Washington, D. C. 20024-2188

W. R. Prindle
1556 Crestline Drive
Santa Barbara, California 93105

A. Schneider
5005 Hidden Branches Drive
Dunwoody, Georigia 30338

THIS PAGE INTENTIONALLY
LEFT BLANK

DISTRIBUTION (cont.)

Number of Copies	
OFFSITE	
1	Ames Laboratory Room 106, Speeding Hall Iowa State University Ames, Iowa 50011-3058 P. Wang
1	Brookhaven National Laboratory Upton, New York 11973 K. Bandyopadhyay
1	Fauske and Associates, Inc. 16W070 W. 83rd Street Burr Ridge, Illinois 60521 H. Fauske
1	Harvard University 295 Upland Avenue Newton Highlands, Massachusetts 02161 M. First
1	Lawrence Livermore National Laboratory P. O. Box 808 Livermore, California 94550 K. Kyle

THIS PAGE INTENTIONALLY
LEFT BLANK

DISTRIBUTION (cont.)

Number of Copies

OFFSITE

5	Los Alamos National Laboratory P. O. Box 1663 Los Alamos, New Mexico 87545	
	S. Agnew	
	R. J. Donohoe	INC-14, MS C345
	S. W. Eisenhawer	
	T. Larson	MS-P915, DX-DO
	L. H. Sullivan	
3	Oak Ridge National Laboratory P. O. Box 2008 Oak Ridge, Tennessee 37831	
	E. Collins	7930, MS-6385
	C. Forsberg	MS-6495
	T. Kress	9108, MS-8088
1	Rice University 5211 Paisley Houston, Texas 77096	
	A. Veletsos	
2	Sandia National Laboratory P. O. Box 5800 Albuquerque, New Mexico 87815	
	D. Powers	6404, MS-0744
	S. Slezak	6415, MS-0741

THIS PAGE INTENTIONALLY
LEFT BLANK

DISTRIBUTION (cont.)

Number of Copies

OFFSITE

1	University of Idaho Chemistry Department Moscow, Idaho 83844-2343 P. Griffiths
1	University of South Carolina Department of Chemistry/Biochemistry Columbia, South Carolina 29208 M. Angel
1	University of Washington Department of Chemistry, BG-10 131 Chemistry Library Bldg. Seattle, Washington 98195 B. R. Kowalski
1	Vanderbilt University P. O. Box 1596, Station B Nashville, Tennessee 37235 F. Parker
2	Westinghouse Savannah River Laboratory P. O. Box 616 Aiken, South Carolina 29802 R. Livingston P. O'Rourke

THIS PAGE INTENTIONALLY
LEFT BLANK

DISTRIBUTION (cont.)

Number of Copies		
ONSITE		
7	U. S. Department of Energy, Richland Field Office	
	D. A. Brown	K8-50
	J. M. Clark	S7-54
	R. E. Gerton	S7-54
	P. R. Hernandez	S7-54
	W. F. Hendrickson	S7-54
	T. Noble	S7-54
	D. E. Trader	K8-50
1	Los Alamos National Laboratory	
	P. G. Eller	S7-53
1	Mactech	
	V. FitzPatrick	K8-50
8	Pacific Northwest Laboratory	
	S. A. Bryan	P7-25
	S. D. Colson	K2-14
	J. S. Hartman	K5-25
	J. H. Lee	B1-40
	P. K. Melethil	P7-22
	A. F. Noonan	K9-81
	R. D. Scheele	P7-25
	G. F. Schiefelbein	P8-38
47	Westinghouse Hanford Company	
	R. Akita	T6-20
	H. Babad	S7-30
	R. A. Bechtold	L0-18

THIS PAGE INTENTIONALLY
LEFT BLANK

DISTRIBUTION (cont.)

Number of Copies

ONSITE

Westinghouse Hanford Company (cont.)

G. N. Boechler	R1-17
D. R. Bratzel	S7-31
R. J. Cash	S7-15
M. D. Crippen	L5-31
D. A. Dodd	T6-50
J. G. Douglas	L5-55
G. T. Dukelow	S7-15
J. B. Duncan	L5-55
S. J. Eberlein	R2-12
R. C. Eschenbaum	N1-21
V. W. Hall	H4-19
C. E. Hanson	H5-09
D. W. Jeppson	L5-31
J. R. Jewett	T6-09
R. E. Johnson	L5-55
T. J. Kelley	S7-30
J. W. Lentsch	S7-15
L. L. Lockrem	S3-90
T. Lopez	L5-55
J. E. Meacham	S7-15
S. J. Mech	L5-55
C. T. Narquis	T6-16
B. L. Philipp	L7-05
R. S. Popielarczyk	R1-30
T. V. Rebagay	T6-30
F. R. Reich (2)	L5-55
D. A. Reynolds	R2-11
G. L. Schutzenhofer	L5-55
J. P. Sederburg	R2-11
T. I. Stokes	H5-09
H. Toffer	H0-38
D. A. Turner	S7-15
W. T. Watson	H0-38
W. D. Winkelman	L5-55
P. A. Young	S7-12

THIS PAGE INTENTIONALLY
LEFT BLANK